CNWRA 2003-XX

NATURAL ANALOGS OF HIGH-LEVEL WASTE CONTAINER MATERIALS— EXPERIMENTAL EVALUATION OF JOSEPHINITE

Prepared for

U.S. Nuclear Regulatory Commission
Contract NRC–02–02–012

Prepared by

G.A. Cragnolino
Y.-M. Pan
D. Turner
E. Pearcy

Center for Nuclear Waste Regulatory Analyses
San Antonio, Texas

August 2003

PREVIOUS REPORTS IN SERIES

Number	Name	Date Issued
CNWRA 91-004	A Review of Localized Corrosion of High-Level Nuclear Waste Container Materials—I	April 1991
CNWRA 91-008	Hydrogen Embrittlement of Candidate Container Materials	June 1991
CNWRA 92-021	A Review of Stress Corrosion Cracking of High-Level Nuclear Waste Container Materials—I	August 1992
CNWRA 93-003	Long-Term Stability of High-Level Nuclear Waste Container Materials: I—Thermal Stability of Alloy 825	February 1993
CNWRA 93-004	Experimental Investigations of Localized Corrosion of High-Level Nuclear Waste Container Materials	February 1993
CNWRA 93-014	A Review of the Potential for Microbially Influenced Corrosion of High-Level Nuclear Waste Containers	June 1993
CNWRA 94-010	A Review of Degradation Modes of Alternate Container Designs and Materials	April 1994
CNWRA 94-028	Environmental Effects on Stress Corrosion Cracking of Type 316L Stainless Steel and Alloy 825 As High-Level Nuclear Waste Container Materials	October 1994
CNWRA 95-010	Experimental Investigations of Failure Processes of High-Level Radioactive Waste Container Materials	May 1995
CNWRA 95-020	Expert-Panel Review of the Integrated Waste Package Experiments Research Project	September 1995
CNWRA 96-004	Thermal Stability and Mechanical Properties of High-Level Radioactive Waste Container Materials: Assessment of Carbon and Low-Alloy Steels	May 1996
CNWRA 97-010	An Analysis of Galvanic Coupling Effects on the Performance of High-Level Nuclear Waste Container Materials	August 1997
CNWRA 98-004	Effect of Galvanic Coupling Between Overpack Materials of High-Level Nuclear Waste Containers—Experimental and Modeling Results	March 1998

PREVIOUS REPORTS IN SERIES (continued)

Number	Name	Date Issued
CNWRA 98-008	Effects of Environmental Factors on Container Life	July 1998
CNWRA 99-003	Assessment of Performance Issues Related to Alternate Engineered Barrier System Materials and Design Options	September 1999
CNWRA 99-004	Effects of Environmental Factors on the Aqueous Corrosion of High-Level Radioactive Waste Containers—Experimental Results and Models	September 1999
CNWRA 2000-06 Revision 1	Assessment of Methodologies to Confirm Container Performance Model Predictions	January 2001
CNWRA 2001-003	Effect of Environment on the Corrosion of Waste Package and Drip Shield Materials	September 2001
CNWRA 2002-01	Effect of In-Package Chemistry on the Degradation of Vitrified High-Level Radioactive Waste and Spent Nuclear Fuel Cladding	October 2001
CNWRA 2002-02	Evaluation of Analogs for the Performance Assessment of High-level Waste Container Materials	March 2002
CNWRA 2003-01	Passive Dissolution of Container Materials—Modeling and Experiments	October 2002
CNWRA 2003-02	Stress Corrosion Cracking and Hydrogen Embrittlement of Container and Drip Shield Materials	October 2002
CNWRA 2003-05	Assessment of Mechanisms for Early Waste Package Failures	March 2003
In Review	Effect of Fabrication Processes on Materials Stability—Characterization and Corrosion	June 2003

ABSTRACT

Analogs can be used to enhance confidence in the performance assessment models for the proposed high-level waste repository at Yucca Mountain, Nevada. Alloy 22, the alloy selected by the U.S. Department of Energy as the outer container material for the waste package, has existed only for slightly more than 20 years and depends on a protective oxide film for its corrosion resistance. It has been suggested that natural metal analogs that have survived for an extraordinarily long time could be useful to reduce concerns regarding the validity of long-term extrapolations when slow uniform corrosion is assumed. This investigation was conducted to assess the validity of josephinite, a rock containing a naturally occurring nickel-iron alloy, as an appropriate natural metal analog. The anodic behavior of josephinite in a simulated groundwater was compared to that of a cast Ni_3Fe alloy using cyclic potentiodynamic polarization and potentiostatic tests to establish the environmental conditions leading to passivity. Minor differences between the sample of josephinite used in this study and the synthetic alloy were found. Josephinite exhibited passivity at a higher pH than did the synthetic alloy and was found to be slightly more susceptible to pitting corrosion. The passive surface layers formed on the josephinite and the cast Ni_3Fe alloy were studied using x-ray photoelectron spectroscopy, and it was found that both passive films have a duplex structure consisting of an iron-rich hydroxide outer layer and a nickel-rich oxide inner layer. It was concluded that passivity alone does not seem to provide an explanation for the survivability of the josephinite sample. The relationship between the passive behavior and the formation of the alteration layers needs to be established for assessing the survivability of josephinite.

CONTENTS

FIGURES

FIGURES (continued)

TABLES

ACKNOWLEDGMENTS

This report was prepared to document work performed by the Center for Nuclear Waste Regulatory Analyses (CNWRA) for the U.S. Nuclear Regulatory Commission (NRC) under Contract No. NRC–02–02–012. The activities reported here were performed on behalf of the NRC Office of Nuclear Material Safety and Safeguards, Division of Waste Management. This report is an independent product of the CNWRA and does not necessarily reflect the view or regulatory position of the NRC.

The authors acknowledge the important contribution of N. Sridhar in the initial phases of this project and are thankful to Professor J. Bird for providing the sample of josephinite used in this study and useful insights on its source. The authors also acknowledge D.S. Dunn for technical review, B. Sagar for programmatic review, and C. Cudd, B. Long, and J. Pryor for editorial reviews. The authors thank J. Gonzalez for assistance in preparing this report.

QUALITY OF DATA: Sources of data are referenced in each chapter. CNWRA-generated laboratory data contained in this report meet quality assurance requirements described in the CNWRA quality assurance manual. Data from other sources, however, are freely used. The respective sources of non-CNWRA data should be consulted for determining levels of quality assurance. Experimental data have been recorded in CNWRA Scientific Notebooks 539 and 557.

ANALYSES AND CODES: No codes were used in the analyses contained in this report.

EXECUTIVE SUMMARY

The Total-system Performance Assessment code is used by the U.S. Nuclear Regulatory Commission to probe the U.S. Department of Energy (DOE) safety case and identify the factors important to performance. It is recognized, however, that a multiple lines of evidence approach is necessary to increase confidence in performance assessment calculations. As part of this approach, natural and archeological analogs have been considered appropriate instruments for increasing understanding and building confidence. Further, the potential use of analogs to provide a technical basis for performance assessment models has been included as part of the requirements for performance assessment in 10 CFR Part 63 [§63.114(g)].

Natural, archeological, and industrial metal analogs were evaluated in a previous report in this series for their applicability to the assessment of container life. Because Alloy 22, the alloy selected by DOE as the outer container material for the waste package at the proposed repository at Yucca Mountain, Nevada, has existed only for slightly more than 20 years and its corrosion behavior is highly dependent on the interplay between material microstructure and environmental conditions, it was concluded that the direct use of analogs in estimating container life is not possible. However, because nickel-chromium-molybdenum alloys depend on a protective oxide film for their corrosion resistance, it has been suggested that natural metal analogs that have survived for an extraordinarily long time could be useful to reduce concerns regarding the validity of long-term extrapolations when slow uniform corrosion (passive dissolution) is assumed. Josephinite, a rock containing a naturally occurring nickel-iron alloy, has been identified as an analog deserving further study. Following this suggestion, a limited investigation was performed by DOE (DOE, 2001a).

This CNWRA investigation was conducted to assess the validity of josephinite as an appropriate natural analog using a specific sample of "new" josephinite provided by Professor J. Bird (Cornell University), who collected it in the proximity of Cave Junction, Oregon. The sample of josephinite was characterized using energy-dispersive x-ray analysis as a predominant awaruite phase containing small dispersed particles of a secondary intermetallic phase identified as Ni_3As_2. The exterior surface of the sample was coated with secondary minerals identified by x-ray diffraction as andradite, serpentine mineral lizardite, and the chlorite group mineral clinochlore $(Mg,Al)_6(Si,Al)_4O_{10}(OH)_8$. A prominent crack across the sample was found filled with serpentine, as well as voids and vugs dispersed in the metallic phase.

An objective of this study was to evaluate the anodic behavior of josephinite in a typical carbonated groundwater, characterized by a slightly alkaline pH because of the presence of bicarbonate among other anionic species commonly presented in groundwater, such as Cl^-, NO_3^-, SO_4^{2-}, and F^-. The purpose was to compare the behavior of josephinite with that of a cast Ni_3Fe alloy using cyclic potentiodynamic polarization and potentiostatic tests and establish the environmental conditions leading to passivity. It was found that both josephinite and the synthetic alloy exhibited a well-defined, passive range in simulated groundwater followed by passivity breakdown and the occurrence of pitting corrosion at higher potentials (above a critical pitting potential). Depending on the OH^- to Cl^- molar concentration ratio in the water in contact with the josephinite, passivity could be maintained up to extremely high potentials, unattainable with natural corrosion conditions. For example, at pH levels above 11.0, when that ratio is sufficiently high (i.e., above 5), pitting corrosion of josephinite is almost completely inhibited. At even higher pH levels, the OH^- to Cl^- molar concentration ratio is so high in the simulated groundwater that passivity predominates completely. There were, however, minor differences

between josephinite and the synthetic alloy. Josephinite exhibited passivity at a higher pH than the synthetic alloy, and it was found to be slightly more susceptible to pitting corrosion. By using x-ray photoelectron spectroscopy, it was found the passive surface layers formed on the josephinite and the cast Ni_3Fe alloy have a duplex structure consisting of an iron-rich hydroxide outer part and a nickel-rich oxide inner part. Even though a stable passive film with a definite composition is formed in the josephinite and the cast Ni_3Fe alloy, no evidence was found to support the modeling of the long-term passive behavior of a nickel-chromium-molybdenum alloy on the basis of the point-defect model. For instance, extended evaluation of the josephinite sample did not help to elucidate if voids could have been generated, as postulated in the model, through coalescence of vacancies at the metallic phase-alteration layer interface.

The difficulties confronted in assessing the validity of josephinite as an adequate analog of a passive, corrosion resistant material such as Alloy 22 can be summarized as follows.

(i) Josephinite does not contain chromium, which is the main alloying element conferring passivity to nickel-chromium-molybdenum alloys. Because the main component of the Alloy 22 passive film is a Cr_2O_3-rich barrier layer, analyses regarding the long-term stability of passive films using josephinite have limitations.

(ii) Although many aspects regarding the origin and formation of josephinite can be inferred, and some are still the subject of controversy, it is difficult or almost impossible to elucidate the evolution of the environments contacting josephinite during its formation.

(iii) Many aspects of the location at which the josephinite was collected are known and, among them, the approximate composition of waters in the region. This information is limited for evaluating the environments contacting the josephinite sample in the location in which it was collected.

The four main benefits of the present study related to the validity of josephinite as an adequate analog are

(i) Characterization of the josephinite sample predominantly an awaruite phase, containing Ni_3As_2 as a minor secondary phase, and covered by a serpentine alteration layer in its outer surface

(ii) Definition of the environmental conditions using pH and groundwater composition, which leads to the passivity of josephinite and the synthetic nickel-iron alloy, and definition of the electrochemical conditions that may promote localized corrosion

(iii) Characterization of the passive film formed on josephinite and the synthetic nickel-iron alloy in simulated groundwater at alkaline pH levels

(iv) Lack of evidence regarding the presence of chlorides in the voids of the josephinite sample, as a means to evaluate the possibility of localized corrosion processes.

It is suggested the alteration layers found on the outside surface of the josephinite sample may have contributed substantially to the preservation and survival of the metallic core. The relationship between the passive behavior of the metal surface and the formation of the alteration layers needs to be established for assessing the survivability of josephinite.

1 INTRODUCTION

The Total-system Performance Assessment code is used by the U.S. Nuclear Regulatory Commission to probe the U.S. Department of Energy (DOE) safety case and identify the factors important to performance (Mohanty, et al., 2000). It is recognized, however, that confidence on performance assessment calculations can be increased by auxiliary analyses based on multiple lines of evidence. The multiple lines of evidence approach uses independent process-level models, abstracted models, sensitivity analyses, observations from laboratory experiments and field service, and natural and archeological analogs to support the models and results of performance assessment calculations. Use of natural analogs has been endorsed by the Nuclear Waste Technical Review Board as a pillar of the repository safety case, independent of performance assessment calculations (Nuclear Waste Technical Review Board, 2001). The joint Nuclear Energy Agency–International Atomic Energy Agency Peer Review of the Total System Performance Assessment for the Site Recommendation states that natural analogs should receive more prominent attention as instruments for increasing understanding and building confidence (Organization for Economic Co-Operation and Development/Nuclear Energy Agency-International Atomic Energy Agency, 2002). Finally, the potential use of analogs to provide a technical basis for performance assessment models has been included as part of the requirements for performance assessment in 10 CFR Part 63 [§63.114(g)].

The application of natural, archeological, and industrial metal analogs for increasing confidence on the assessment of waste package performance was evaluated in a previous report (Sridhar and Cragnolino, 2002). The report was to review the literature related to corrosion of metal analogs and assess the information available to increase the confidence on container life estimations. It was noted that, even though natural and archeological analogs have been used in buttressing the case for the performance of engineered barriers in radioactive waste disposal programs (Johnson and Francis, 1980)[1], using these analogs for estimates of container life (e.g., deriving a corrosion rate from analog studies) is plagued with difficulties. Also, natural analogs, and, in particular, archeological analogs, may constitute a biased sample because similar objects could have completely corroded away and are not available anymore, except in cases where the history of the entire collection of buried artifacts is known and the survivability can be assessed (Miller, et al., 2000).

Because of the type of alloys proposed to be used as container materials for the alternating wet and dry and oxidizing conditions anticipated at the proposed Yucca Mountain repository horizon, thermodynamic immunity is not expected. Instead, the corrosion resistance of nickel-chromium-molybdenum alloys, such as Alloy 22, depends on the presence of a protective oxide film on the alloy surfaces through which slow uniform corrosion (passive dissolution) occurs. Corrosion is seldom continuous or linear and may be dictated by threshold conditions of potential, temperature, or environmental factors where one corrosion mode may be replaced by another. In certain conditions, for example, breakdown of passivity may lead to localized corrosion in the form of pitting or crevice corrosion, implying significantly higher corrosion rates in localized areas of the metal surface. Predicting corrosion rates requires an accurate

---

[1]David, D., D. Crusset, and C. Lamaitre. "Archeological Analogues Studies for the Prediction of Long-Term Corrosion on Buried Metals." International Workshop on Long-Term Corrosion Behavior in Nuclear Waste Systems, Cardarache, France, November 26–29, 2001. Cardarache, France. In press. 2001.

knowledge of the material condition (chemical composition, microstructure, thermomechanical history, geometry, and such) and the contacting environment (anionic and cationic concentrations, redox potential, temperature, fluid flow, and such). Either or both these knowledge bases are usually missing in analog studies. Additionally, even if the environmental and material parameters can be reasonably estimated, the corrosion morphology of the available metal analogs can be different from that of the waste package materials. Finally, the alloys being considered by DOE for containers have been in existence for only a few decades. Similar corrosion resistant materials, such as stainless steels, have been in existence for approximately 75 years. Nickel-base alloys similar to Alloy 22 have been developed and used only in the last 30 years.

1.1 DOE Assessment of Josephinite As a Natural Analog

DOE has evaluated a variety of natural and archeological analogs to increase the confidence on the estimations of the long-term waste package performance (DOE, 2001b; CRWMS M&O, 2002). Among many cases discussed, the preservation of various archeological objects in Egyptian pyramids and tombs and bronze objects in caves located in an arid zone in Israel has been cited as evidence the corrosion rate of metallic materials can be low in natural and human-made openings located in the unsaturated zone. Another example cited by DOE (2001b) refers to iron objects, in this case, buried in a river-flood plain, a completely wet environment. A large number of iron nails were discovered buried in an ancient Roman site in Scotland. Whereas the nails near the surface corroded entirely, the nails deeper inside the hoard have remained intact for approximately 2,000 years. Although DOE attributed the relative preservation of the nails deep inside the hoard to the protective nature of the corrosion crust formed by the outer layer of nails, it is likely the consumption of oxygen by the outer layer of nails created a reducing environment inside the hoard that helped prevent corrosion (Miller, et al., 2000; Sridhar and Cragnolino, 2002). These two examples reveal certain advantages of archeological objects as illustrations of the expected long-term behavior of metals; however, the lack of detailed information on the environmental conditions is a real limitation in their use as analogs.

DOE also has conducted an evaluation and examined a sample of josephinite, a rock that contains the intermetallic mineral awaruite, which is an ordered phase with stoichiometry of Ni_3Fe (DOE, 2001a; CRWMS M&O, 2002). The age and geologic history of the josephinite sample are not known. It had a significant metallic luster, even though the sample was found in a river bed, and it is not known for how long it was exposed to the water. The nominal composition was found to be 72.43-atomic percent nickel and 27.57-atomic percent iron. The sample was subjected to surface analysis by x-ray photoelectron spectroscopy, which is capable of detecting the oxidation state of elements on the surface (DOE, 2001a). By sputtering the sample with an argon ion beam, a depth profile of species was obtained. The analysis suggested the presence of metallic nickel and iron in the metallic and oxidized states (presumably Fe_3O_4, Fe_2O_3, or both oxides). Metallic nickel, however, was not detected on the surface, and the valence state of iron in the oxide was not determined. It was claimed the small difference between the binding energies for Fe(II) and Fe(III) made this distinction difficult. During sputtering, the average nickel-to-iron atomic ratio was found to be approximately equal to 3.4, which is consistent with the composition of awaruite. Significant out-gassing was noted, making it difficult to attain sufficient vacuum to perform the x-ray photoelectron spectroscopy analyses. This out-gassing was attributed to a high porosity related to a large quantity of voids in the black surface layer, the bulk volume of the mineral, or both. The observation of metallic

nickel and iron (in unknown, but small quantities) was suggested as evidence that more corrosion resistant alloys containing chromium and molybdenum, such as Alloy 22, may survive for even longer periods of time. It must be noted, however, that any conclusion relative to the lifetime or corrosion rate from this initial investigation by DOE is suspect for a number of reasons: (i) the age and geochemical exposure conditions are unknown; (ii) although surface analysis by x-ray photoelectron spectroscopy may indicate presence of metallic species, it provides no evidence regarding the extent of prior dissolution; and (iii) no conclusions can be made regarding the corrosion mechanisms. In conclusion, the study is too limited to reach a definite conclusion regarding the reasons for the survivability of the josephinite sample, not only because its geochemical history and age are unknown, but also because of the restricted scope of this investigation.

1.2 Evaluation of a Josephinite Sample at CNWRA

Although josephinite does not contain the alloying elements, chromium and molybdenum (and tungsten), which confer passivity and high localized corrosion resistance to Alloy 22, it was suggested worthwhile (Sridhar and Cragnolino, 2002) to conduct an experimental study to investigate the mechanism responsible for conferring corrosion resistance to this natural metallic material. The rationale behind this suggestion was that a natural analog such as josephinite would be useful to increase the confidence in process level or mechanistic models, in this case related to the long-term passive behavior, if additional studies could shed light on certain aspects of the corrosion processes and mechanisms. It was hypothesized that the apparent long-term stability of josephinite metal may be explained by the presence of minor alloying elements, which lend it a specific electrochemical response resulting in long life, or the near-field environment surrounding the josephinite providing conditions for thermodynamic immunity or slow corrosion kinetics or some combination.

Experimental studies conducted at the Center for Nuclear Waste Regulatory Analyses using a sample of josephinite provided by Professor J. Bird are described in this report. The report is structured as follows. In Chapter 2, a description of josephinite as a naturally occurring metal is provided, in which the geological and geochemical conditions of its occurrence are discussed. Hypotheses regarding the origins of josephinite are briefly summarized as are its general characteristics. Finally, a description of the josephinite sample used in this study is presented. The electrochemical behavior of josephinite in simulated groundwater environments is described in Chapter 3. In this chapter, the electrochemical response of a synthetic nickel-iron alloy with a chemical composition similar to that of josephinite is presented for comparison and the passive behavior of both materials is discussed. Chapter 4 contains a detailed characterization using x-ray photoelectron spectroscopy of the passive layers formed on josephinite and the synthetic nickel-iron alloy. The validity of josephinite as a natural analog is discussed in Chapter 5. The summary, conclusions, and recommendations for future activities arising from this study are included in Chapter 6. References are listed in Chapter 7.

2 JOSEPHINITE AS A NATURALLY OCCURRING METAL

Josephinite that contains nickel-iron minerals has been identified as a natural analogue for the assessment of container life. In this chapter, a description of the geological and geochemistry conditions, hypotheses of the origins, and the general characteristics of josephinite is provided. Characterization of a sample of josephinite using scanning electron microscopy, energy-dispersive x-ray analysis, and x-ray diffraction is also reported.

2.1 Geological and Geochemical Conditions

Josephinite, a rock containing a naturally occurring nickel-iron alloy, was first identified and described by Melville (1892). The bulk of the samples, including the original samples reported by Melville (1892), are mechanically weathered pebbles and nuggets collected from placer gravel deposits in Josephine Creek in Josephine and Jackson Counties in southwestern Oregon. As reported by Melville (1892), the samples consist of approximately 60-wt% nickel, 27-wt% iron, and 12-wt% silicate material. Melville (1892) also reported trace amounts of chromium, arsenic, and cobalt. Josephinite nuggets range from 1 to 10 cm [0.39 to 3.94 in] in diameter. There are references to *in-situ* samples of the nickel-iron mineral awaruite (Ni_3Fe) that are typically much smaller, on the order of 100 µm [3.9 mils] or less (Botto and Morrison, 1976).

The location for josephinite is in gravel deposits along Josephine Creek where it cuts through intensely sheared and serpentinized peridotites at the base of the Josephine Peridotite (Dick, 1974). The peridotite, part of the Josephine Ophiolite complex, is contained in a thrust sheet that covers approximately 1,000 km^2 [400 mi^2] in southwestern Oregon and northern California. The Josephine Peridotite is approximately 30 to 40-percent fresh, unaltered harzburgite {olivine [$(Mg,Fe)_2SiO_4$] plus orthopyroxene [$(Mg,Fe)SiO_3$]} and approximately 30-percent mildly serpentinized peridotite. The remaining peridotite is heavily serpentinized and sheared (Dick, 1974; Botto and Morrison, 1976; Ramp and Peterson, 1979).

Of particular interest in the use of josephinite as a natural analog is the period of time it has been exposed to near-surface weathering and the chemistry of the water with which it has come into contact. Some limited isotopic information suggests josephinite crystallized perhaps as much as 1.4 billion years ago (Bird, et al., 1999), but not all of this time was spent at near-surface conditions. Based on potassium-argon age dating of contemporaneous diabase and hornblende diorite dikes, the maximum age of the Josephine Peridotite is estimated at approximately 150–155 million years (Dick, 1973). It is also unlikely that the samples have been exposed to near-surface conditions for this amount of time, but it may be possible to place time constraints based on the ages of the gravel deposits in Josephine Creek and the Illinois River Basin. For example, the terrace gravels of Josephine Creek where josephine nuggets have been found are assigned a Pleistocene age (1.6 million to 800,000 years) by Ramp (1986). Slightly older ages of 6 million years to present are assigned to laterite soil deposits above Josephine Creek, suggesting that the Josephine Peridotite has been exposed to chemical weathering for at least that amount of time (Ramp, 1986).

Barnes, et al. (1967) reported that the presence of high-magnesium ultramafic rocks (peridotites, dunites) produces predominantly Mg^{2+}-HCO_3^- surface and near-surface groundwaters in serpentinite terrains of the western United States. Alteration of the

magnesium-silicate minerals typically results in slightly alkaline (pH > 8) waters that are high in Ca^{2+}, Mg^{2+}, SiO_2(aq), and HCO_3^- and low in Na^+ and Cl^-. Barnes and O'Neil (1969) also reported rare occurrences of alkaline (pH >11) Ca^{2+}-OH^- waters in the Pacific Northwest. These waters are found in springs in incompletely serpentinized ultramafic rocks. Concentrations of Na^+, Cl^-, and SiO_2 are higher and Mg^{2+} and HCO_3^- are much lower than those reported for the more common Mg^{2+} -HCO_3^- waters. Magnesium is most likely removed from these waters by the precipitation of the alteration mineral brucite [$Mg(OH)_2$] (Barnes and O'Neil, 1969).

Water chemistry data are not available for the Josephine Creek watershed, but water quality information is available for the larger Illinois River Basin (U.S. Geological Survey Hydrologic Unit Code 17100311) that includes Josephine Creek. Although there are no current water-sampling activities in the Illinois River Basin, historic water quality data were obtained from the National Water Information Service managed by the U.S. Geological Survey (available at http://waterdata.usgs.gov/nwis/qwdata). The Illinois River sampling location (U.S. Geological Survey Site Number 14377100) closest to Josephine Creek is at Kerby, Oregon, approximately 6.7 km [4.2 miles] upstream from the confluence of the two streams. The average composition for the Illinois River water collected at this site is compared in Table 2-1 to representative water chemistries in the vicinity of Yucca Mountain (CRWMS M&O, 2002). Consistent with the observations of Barnes, et al. (1967), the water from the Illinois River is a dilute Mg^{2+}-HCO_3^- water as compared with the Na^+-HCO_3^- and Ca^{2+}-HCO_3^- waters in the vicinity of Yucca Mountain. The river water is more dilute than Yucca Mountain waters. It is worth noting that the river water has a much lower concentration in key anions such as Cl^- and NO_3^- than both the synthetic unsaturated water and the J–13 Well water (CRWMS M&O, 2002).

2.2 Hypotheses on the Origins of Josephinite

Although almost all reported josephinite samples are from gravel deposits, Dick (1974) reported finding small *in-situ* samples {up to 4 mm [0.2 in]} of josephinite in serpentinite veins at the margins of the shear zone. Based partly on these samples, Dick (1974) equated josephinite with the nickel-iron alloy awaruite. More recently, Bird (2001) has reported finding *in-situ* josephinite several kilometers from the original placer deposits. This "new" josephinite occurs higher in the geologic section, with *in-situ* blocks of up to several kilograms hosted in unaltered harzburgite of the Josephine Peridotite.

The origin of josephinite is controversial. One hypothesis involves the formation of josephinite as a late-stage product of hydrothermal metamorphism and serpentinization of peridotite (Dick, 1974; Dick and Gillette, 1976; Botto and Morrison, 1976). Much of the evidence for this hypothesis is in the close spatial association of josephinite found in Josephine and Mendenhall Creeks with zones of intense shearing and serpentinization of the Josephine Peridotite and N–NE trending dikes. Reducing conditions capable of forming nickel-iron alloys (Frost, 1985) are attributed to serpentinization reactions. For example, reactions such as the serpentinization of iron-rich fayalite olivine

$$\underset{\text{Fe-Olivine}}{6Fe_2SiO_4} + 7H_2O = \underset{\text{Fe-Serpentine}}{3Fe_3Si_2O_5(OH)_4} + \underset{\text{Magnetite}}{Fe_3O_4} + H_2 \qquad (2\text{-}1)$$

release hydrogen gas (H_2) that can act as a reducing agent for either nickel and iron released by the alteration of olivine or for primary nickel-iron sulfide minerals such as pyrrhotite ($Fe_{1-x}S$, with $0<x<2$) and pentlandite $(Fe,Ni)_9S_8$ (Botto and Morrison, 1976; Thornber and

Table 2-1. Chemical Compositions of Waters Related to Yucca Mountain Site and the Illinois River Near Kerby, Oregon

Ionic Species and pH	J–13 Well Water*		Synthetic J–13 Well Water†		Synthetic Unsaturated Water†		Illinois River, Kerby, Oregon‡	
	mg/L	mM	mg/L	mM	mg/L	mM	mg/L	mM
Ca^{2+}	13.0	0.33	5.8	0.15	57.3	1.45	5.9	0.15
Mg^{2+}	2.01	0.08	2.1	0.08	11.8	0.47	10.2	0.40
Na^{+}	45.8	1.99	45.2	1.96	8.56	0.37	1.9	0.08
K^{+}	5.04	0.13	5.2	0.13	4.0	0.10	0.3	0.008
HCO_3^{-}	128.9	2.11	105.0	1.72	20.3	0.33	70.2	1.15
$SiO_2(aq)$	60.9	1.02	10.4	0.17	10.4	0.17	17.4	0.29
Cl^{-}	7.14	0.20	7.2	0.20	76.6	2.14	1.9	0.05
SO_4^{2-}	18.4	0.19	18.5	0.19	83.9	0.87	1.6	0.02
NO_3^{-}	8.78	0.14	7.9	0.12	10.7	0.17	0.3	0.005
F^{-}	2.18	0.11	2.3	0.12	2.2	0.11	0.04	0.002
pH	7.41	—	8.07	—	7.55	—	7.73	—

*CRWMS M&O, 2000 (from Harrar, J.E., J.F. Carley, W.F. Isherwood, and E. Raber. "Report to the Committee to Review the Use of J–13 Well Water in Nevada Nuclear Waste Storage Investigations." UCRL–ID–21867. Livermore, California: Lawrence Livermore National Laboratory. 1990).
†CRWMS M&O, 2002 (from Rosenberg, N.D., G.E. Gdowdski, and K.G. Knauss. "Evaporative Chemical Evolution of Natural Waters at Yucca Mountain, Nevada." *Applied Geochemistry.* Vol. 16. pp. 1,231–1,240. 2001).
‡Average of six samples collected from USGS site number 14377100 on the Illinois River between January 1963 and March 1971 (http://waterdata.usgs.gov/nwis/qwdata).

References:

CRWMS M&O. "Natural Analogue Synthesis Report." TDR–NBS–GS–00026. Rev. 00 ICN02. Las Vegas, Nevada: CRWMS M&O. 2002.

CRWMS M&O. "Environment on the Surfaces of the Drip Shield and Waste Package Outer Barrier." ANL–EBS–MD–000001. Rev 00 ICN 01. Las Vegas, Nevada: CRWMS M&O. 2000.

Haggerty, 1976). In addition to iron, other metals such as nickel, cobalt, and copper that are possibly present in minor quantities in the peridotite could be liberated during alteration and deposited along a reducing serpentinization front. Dick (1974) reported that an absence of associated sulfide minerals suggests the mineral awaruite found in josephinite most likely formed through direct reduction of nickel and iron liberated during serpentinization of mafic minerals such as olivine and pyroxene. Small flecks of josephinite that occur at the margins of zoned serpentinite veins and in the adjacent harzburgite are used to support the serpentinization hypothesis (Dick, 1974). The low concentrations of nickel in the silicate minerals that make up the peridotite suggest that its availability would be a limiting factor in the formation of josephinite according to this hypothesis (Dick, 1974).

As part of this hypothesis, Botto and Morrison (1976) proposed that a reducing, calcium-rich hydrothermal solution at an advancing serpentinization front could further react with peridotite components to produce mineralogies similar to those observed in josephinite. For example, the alteration of diopside and olivine

$$\underset{\text{Diopside}}{3CaMgSi_2O_6} + \underset{\text{Olivine}}{9Mg_{1.67}Fe_{0.33}SiO_4} + 12H_2O = \underset{\text{Mg-Serpentine}}{6Mg_3Si_2O_5(OH)_4} + \underset{\text{Andradite}}{Ca_3Fe_2Si_3O_{12}} + \underset{\text{Native Iron}}{Fe} \quad (2\text{-}2)$$

could account for the association of andradite, serpentinite, and native iron. Bird and Weathers (1979), however, indicate that this reaction could occur only at temperatures too low {<400 °C [750 °F]} for large-scale serpentinization. They also reported that, although andradite and nickel-iron alloys are closely associated in josephinite, serpentinite consistently postdates andradite.

A second hypothesis calls for the formation of josephinite at high pressures and temperatures at depth, perhaps as deep as the D″ layer {2,700 km [1,600 mi]} near the core-mantle boundary (Bird and Weathers, 1975, 1979; Bassett, et al., 1980; Bird, et al., 1999; Bird, 2001). The josephinite was then transported into the lithosphere by a deep-mantle plume and emplaced in the crust by the obduction of the ophiolite sequences associated with the Josephine Peridotite onto the continental crust. Proponents of the deep-mantle hypothesis use textural relationships to suggest that the nickel-iron alloys formed at high temperatures and preceded magnetite and serpentinite in the paragenetic sequence. The lack of early sulfide minerals is also used to argue for an origin of josephinite that precedes the serpentinization of the Josephine Peridotite (Bird and Weathers, 1975, 1979). A second focus of this hypothesis is distinguishing the nickel-iron alloys in josephinite as being different from the ordered awaruite phase. Bird and Weathers (1975) also suggest that the large size and the lower nickel content (less than 75 atomic percent) of josephinite nuggets indicate that josephinite is different from the awaruite reported by Dick (1974) as forming by reduction during serpentinization. Additional information used to support the deep-mantle hypothesis includes the recent finding of large *in-situ* samples of josephinite in unaltered harzburgite (Bird, 2001) and data that suggest josephinite has noble gas and osmium and lead isotopic signatures similar to values expected for the core–mantle transition zone (Downing, et al., 1977; Bochsler, et al., 1978; Bird, et al., 1999).

2.3 General Characteristics of Josephinite

Although classified in some instances as a mineral equivalent to awaruite (Ramdohr, 1950; Dick, 1974), there is consensus that josephinite is a rock (Melville, 1892; Bird and Weathers,

1975, 1979; Botto and Morrison, 1976; Bassett, et al., 1980). The following is a brief summary of minerals reported in josephinite.

2.3.1 Nickel-Iron Intermetallic Phases

Botto and Morrison (1976) noted a bimodal distribution of nickel-iron minerals in josephinite. These minerals include regions where the nickel content is 73–75 atomic percent, consistent with the ordered phase awaruite. A second metallic phase has nickel content of 62–66 atomic percent, similar to the disordered phase taenite (Botto and Morrison, 1976). Based on scanning electron microscope and transmission electron microscope studies, Bassett, et al. (1980) observed awaruite and also wairuite (FeCo) as exsolution lamellae in the metallic phases of josephinite. As a result of textures observed in josephinite pebbles, Botto and Morrison (1976) reported a zonation of the metal alloys, from inner zones with approximately equal amounts of awaruite and taenite, with taenite decreasing outward.

Other metallic phases observed in josephinite include rare nickel arsenide (Ni_3As_2) blebs, native copper, gold, and magnetite (Botto and Morrison, 1976). Copper occurs both syngenetic with the nickel-iron alloy and as a late-stage phase crosscutting all other phases. Gold is rare and occurs as late-stage blebs cross cutting the nickel-iron alloys. Magnetite occurs as rounded blebs and millimeter-sized inclusions in the alloys, and textural relationships suggest it is a late-stage replacement of the early metallic phases (Bird and Weathers, 1975).

2.3.2 Associated Silicate Phases

In addition to the nickel-iron alloys, andradite garnet ($Ca_3Fe_2Si_3O_{12}$) is commonly observed to form intimate intergrowths as a primary mineral phase (Dick, 1974; Botto and Morrison, 1976). Based on its occurrence forming a central zone in many josephinite samples and other textural evidence, the assemblage andradite + nickel-iron alloy is typically identified as forming early in the paragenetic sequence. Other early silicate minerals include accessory magnesium silicates such as diopside pyroxene ($CaMgSi_2O_6$) (Botto and Morrison, 1976), forsterite olivine (Mg_2SiO_4), and enstatite pyroxene ($MgSiO_3$).

Textural and crosscutting relationships (Bird and Weathers, 1979) suggest that serpentine + magnetite postdate the earlier andradite + nickel-iron alloy + Mg-silicates. Serpentine group minerals [$Mg_3Si_2O_5(OH)_4$] include lizardite, antigorite, chrysotile, and the Ni-serpentinite garnierite (Bird and Weathers, 1975; Botto and Morrison, 1976). Serpentine typically occurs as an exterior coating of josephinite pebbles along with magnetite and copper (Botto and Morrison, 1976). Serpentine also occurs in veins that cut across earlier mineral assemblages. Massive antigorite tends to form the outer skin on josephinite pebbles, and bladed chrysotile forms the vein-filling material (Botto and Morrison, 1976).

2.4 Description of the Josephinite Sample at CNWRA

A sample of josephinite, designated as JS–JB1, was obtained from Professor J. Bird (Cornell University). The sample was cut as a slide from a larger mass of *in-situ* "new" josephinite. The cut face of the sample, exhibiting a metallic luster, is shown in Figure 2-1. A long crack that

Figure 2-1. View of the Cut Face of the Josephinite Sample JS–JB1 Showing Its Metallic Appearance. A Long Crack Is Clearly Visible on the Left Side of the Sample. (Scale in Inches, 1 in = 25.4 mm)

extends from the top to the bottom of the sample is clearly visible on its left side. The sample was collected on June 11, 1999, approximately 8 km [5 mi] southwest of Cave Junction, Oregon, as shown on the map in Figure 2-2.[2]

A small portion of the sample, designated JS–JB1–S1, was cut from the bottom left corner, across the major crack, as shown schematically in Figure 2-3, to conduct a more detailed examination. The exterior surface of the sample, coated with secondary minerals exhibiting reddish-orange colors, is shown in Figure 2-4, after the cutting of the subsample JS–JB1–S1. A portion of the alteration material covering the sample of josephinite was removed using a steel pick and crushed in a mortar and pestle to conduct energy-dispersive x-ray analysis in the scanning electron microscope and x-ray diffraction analysis. The energy-dispersive x-ray analysis spectrum shows peaks that correspond mostly to magnesium, silicon, oxygen, and calcium, some aluminum and iron, and minor nickel (Figure 2-5). The weight percent and the

---

[2]Bird, J.M. Personal communication (August 19) to N. Sridhar, CNWRA. Ithaca, New York: Cornell University. 2002.

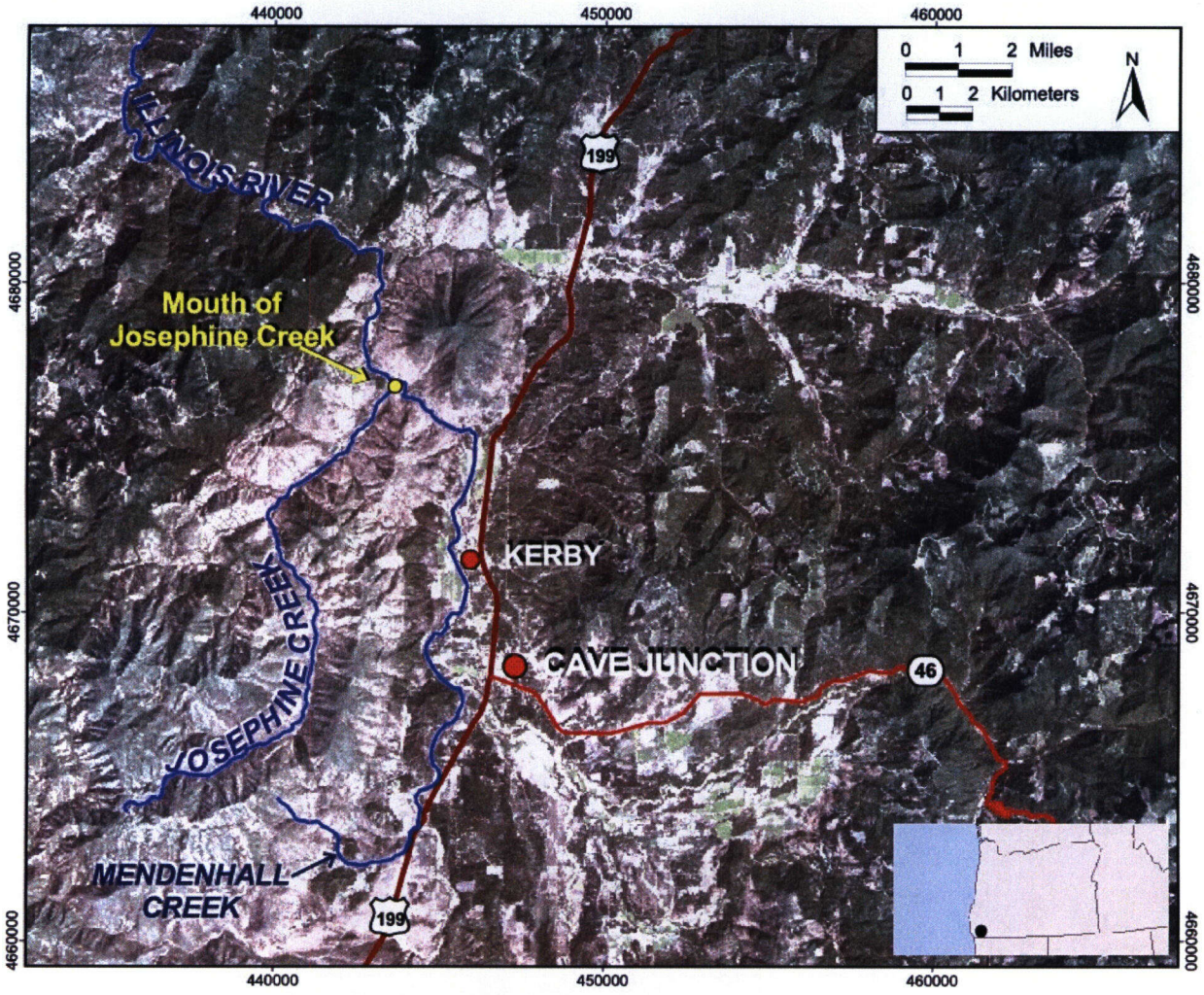

Figure 2-2. Map of Josephinite Creek Near Cave Junction, Josephine County, Oregon. Universal Transverse Mercator, Zone 10N; Map Datum: World Geodetic System 1984; Vector Data Source: Environmental Systems Research Institute; Background Image: Subset of a Landsat Thermal Mapper Image, Path 046/Row 31, September 3, 1989; Satellite Data Courtesy of Global Land Cover Facility, University of Maryland.

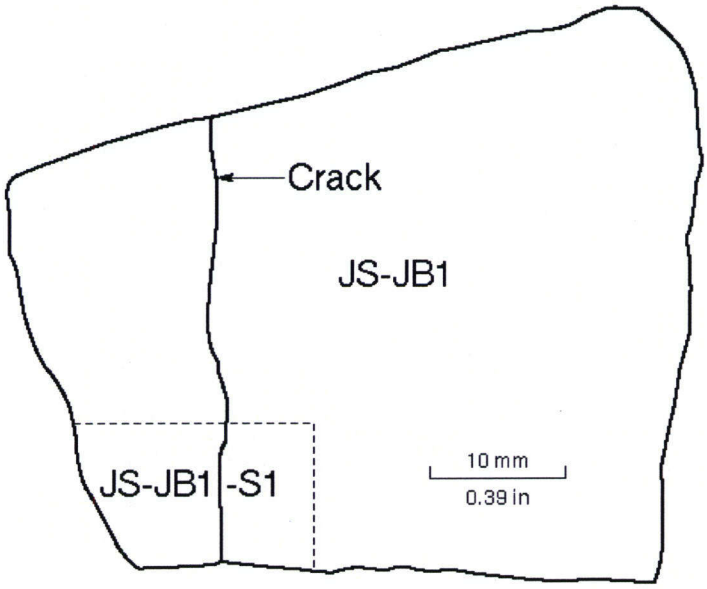

Figure 2-3. Schematic Drawing of the Josephinite Sample JS–JB1 Showing the Position Selected for Cutting Subsample JS–JB1–S1

Figure 2-4. View of the Outer Surface of the Josephinite Sample JS–JB1 After Cutting Subsample JS–JB1–S1 (Scale in Inches, 1 in = 25.4 mm)

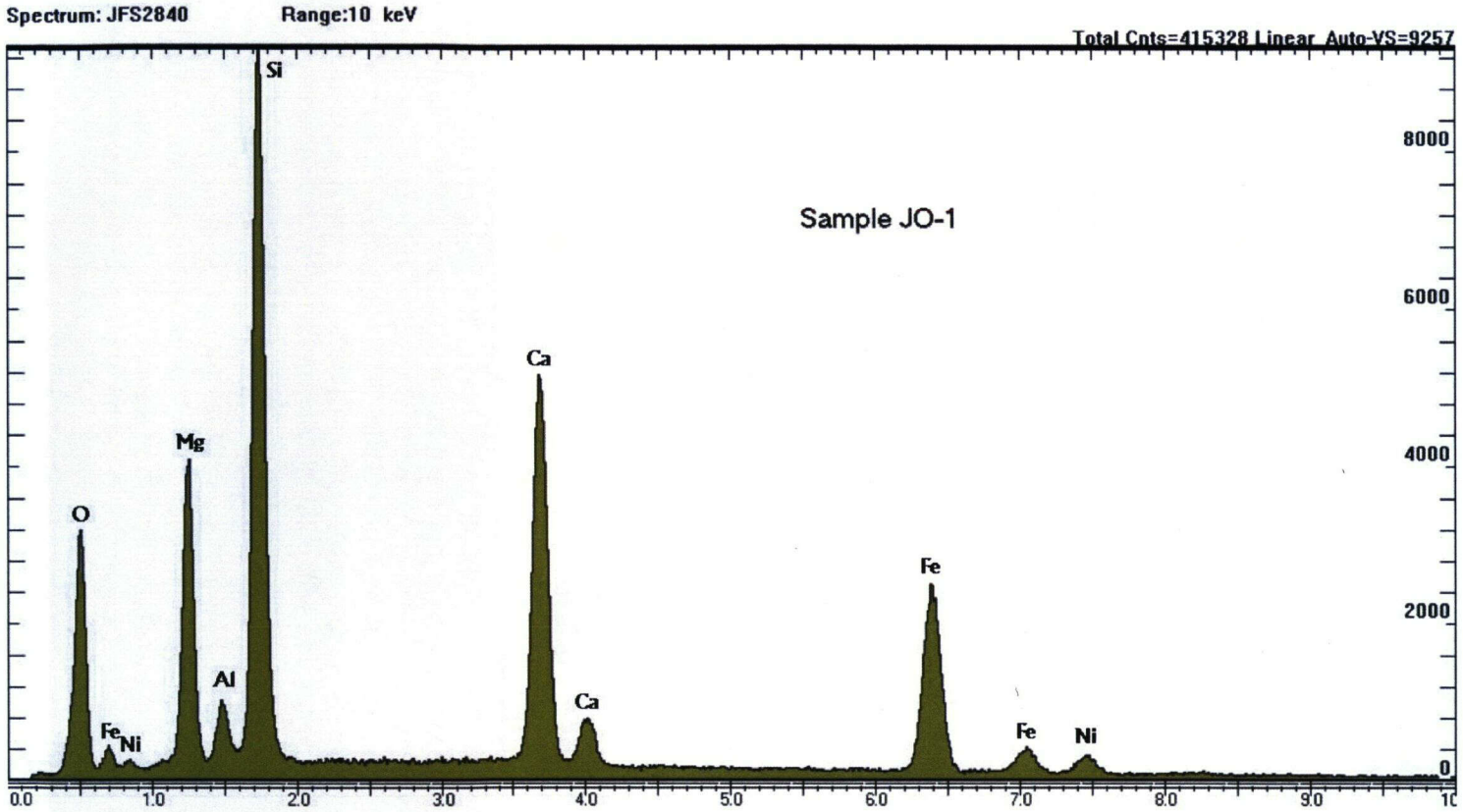

Figure 2-5. Energy-Dispersive X-Ray Spectrum of the Alteration Material Covering the Outer Surface of Josephinite Sample JS–JB1Figure 5

atomic percent content of these elements in the coating is reported in Table 2-2. Although oxygen appeared in the spectrum, the values reported in Table 2-2 do not include its content because the analysis of oxygen was only semiquantitative as a result of the reduced sensitivity associated with the low-energy end of the spectrum. The most likely phases that match the observed x-ray diffraction analysis spectrum include, as shown in Figure 2-6, andradite garnet, the serpentine mineral lizardite, and the chlorite group mineral clinochlore $(Mg,Al)_6(Si,Al)_4O_{10}(OH)_8$.

Table 2-2. Scanning Electron Microscope–Energy-Dispersive X-Ray Analysis of the Alteration Coating in Josephinite Sample JS–JB1

Element	Weight Percent	Atomic Percent
Magnesium	16.48	22.87
Aluminum	3.65	4.57
Silicon	32.43	38.96
Calcium	21.19	17.84
Iron	22.86	13.81
Nickel	3.38	1.94

Two polished thin sections of the subsample JS–JB1–S1 were examined by optical microscopy using both reflected and transmitted light. The composed optical image for subsample JS–JBI–S1–TS2 is shown in Figure 2-7. The coating on the exterior surface ranges from 0 to approximately 0.6 mm [0 to 0.02 in] in thickness and consists of thin laminations of serpentine minerals oriented in layers subparallel to the outside surface. The coating also includes clusters of small {10–20 mm [0.4–0.8 mils]} equant crystals of andradite adjacent to the josephinite. Beneath this coating, the surface of the josephinite is highly irregular with numerous embayments up to approximately 80 mm [3.1 mils] deep, with small euhedral andradite garnet crystal. Fragments of josephinite separated from the main underlying mass occur only rarely within the coating. The coating does not appear to be direct alteration from the underlying josephinite, and transitional phases are not apparent at the resolution of the optical microscope.

The portion of the crack shown in subsample JS–JB1–S1–TS2 (Figure 2-7) has a width of 20 to 150 mm [0.8 to 5.9 mils] and is filled with serpentinite minerals. The crack appears to have formed as a mechanical brittle fracture with minimal deformation. Some dissolution may have occurred along the fracture, but the crack walls match closely. The degree of corrosion of the crack walls seems to be more pronounced in location 1, which is the more distant from the outside surface of the sample, as shown in Figure 2-8 for the two locations indicated in Figure 2-7. It should be noted by examining Figure 2-1 that the external surface in subsample JS–JB1–S1–TS2 corresponds to the end of the crack extension across the original JS–JB1 sample. There are no obvious changes in the mineralogy of the crack-filling material

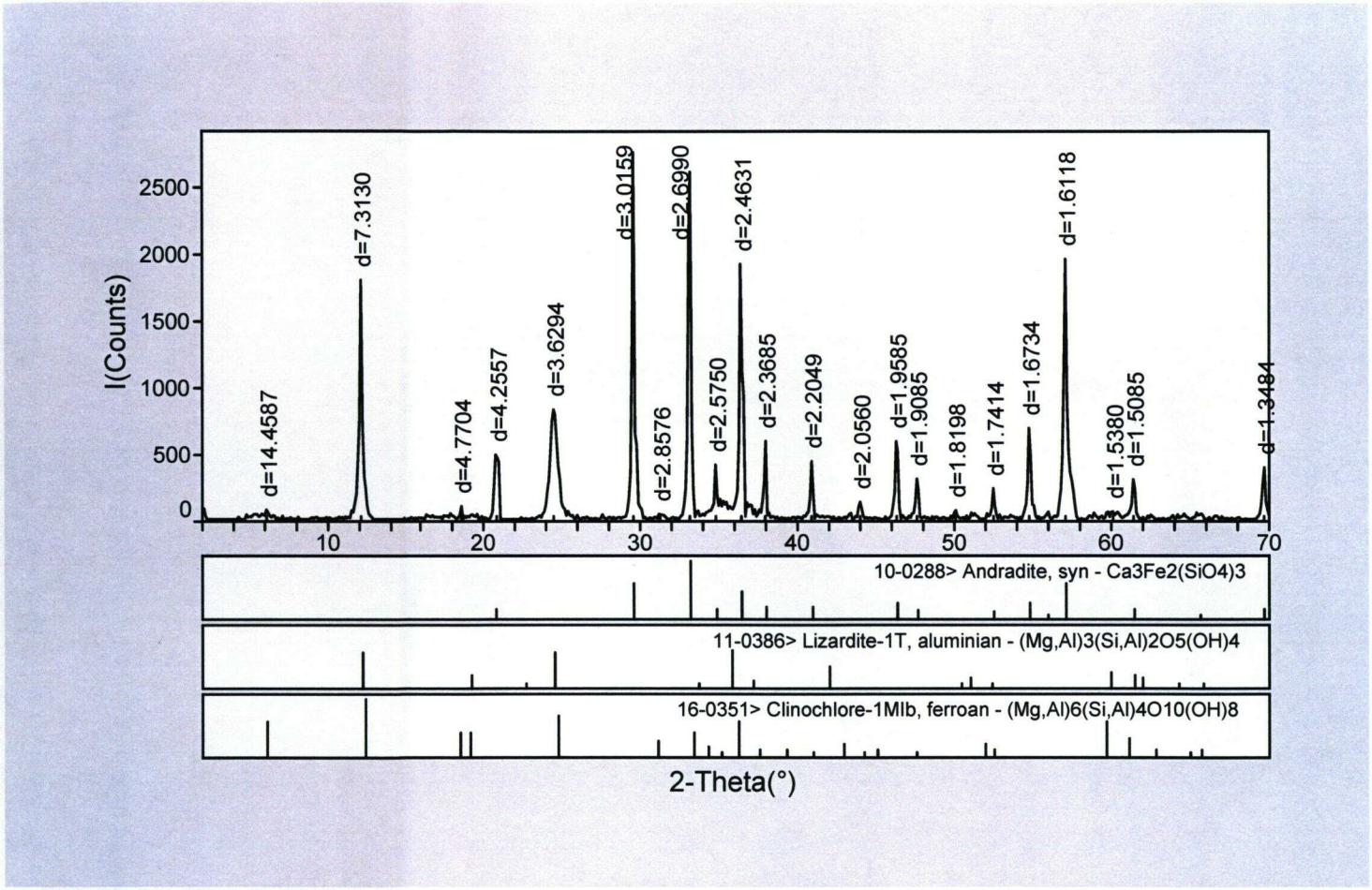

Figure 2-6. X-Ray Diffraction Spectrum of the Alteration Material Covering Outer Surface of Josephinite Sample JS–JB1

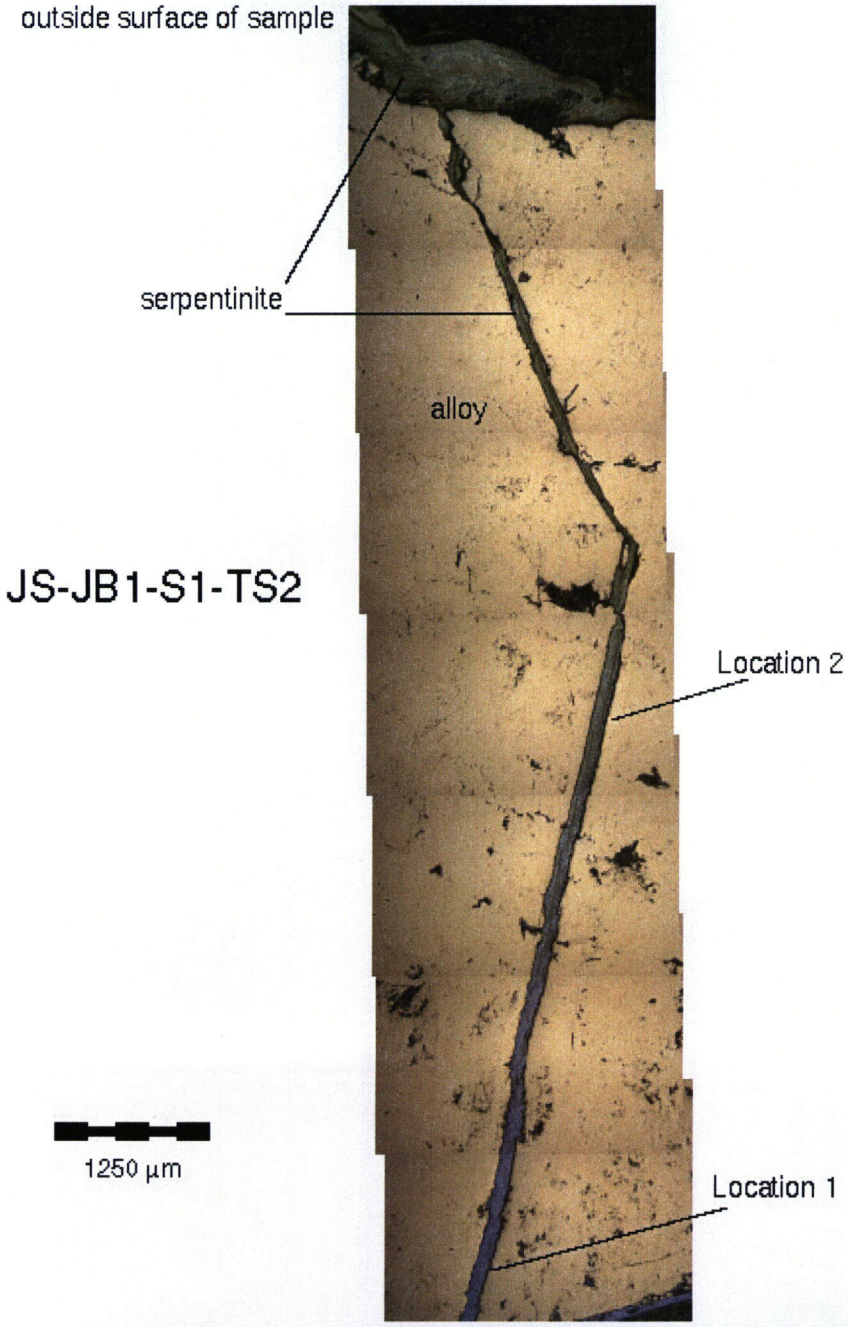

Figure 2-7. Composed Optical Micrograph of a Polished Thin Section of Subsample JS–JB1–S1 Showing Locations of Energy-Dispersive X-Ray Analyses Along the Crack Shown in Figure 2-1
{Location 1 is 9 mm [0.4 in] from Outside Surface, Location 2 is 5 mm [0.20 in] from Outside Surface, 1,250 µm = 49 mils}

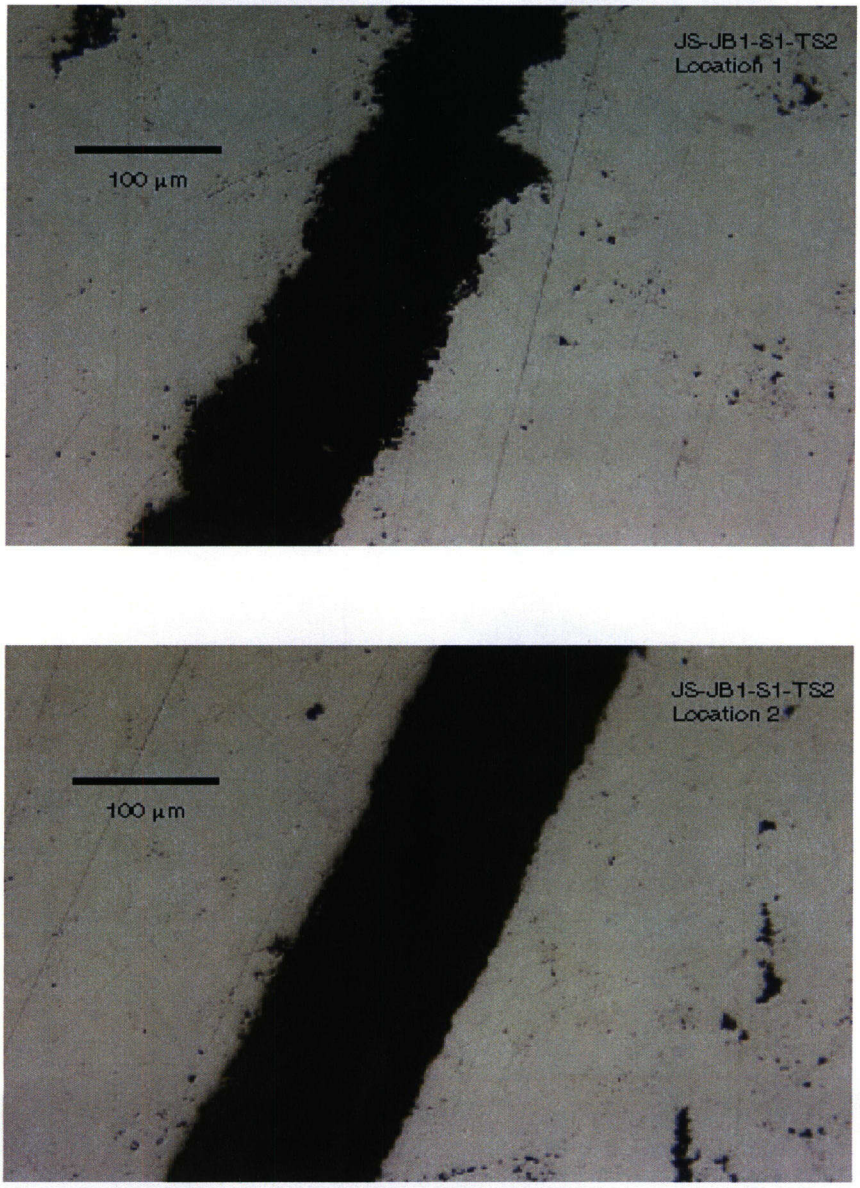

Figure 2-8. High Magnification Optical Micrographs of Two Locations Along the Crack in Subsample JS–JB1–S1 Shown in Figure 2-7 (100 µm = 3.9 mils)

with crack depth, and the layered serpentinite minerals that fill the crack tend to be oriented at high angles to the fracture walls.

Scanning electron microscope–energy-dispersive x-ray analysis was also used to analyze the crack-filling material and the alloy composition along a trace perpendicular to the crack at two locations. The locations chosen were approximately 5 mm [0.2 in] and 9 mm [0.4 in] from the outer surface of the original sample, as indicated in Figure 2-7. The prevailing elements of the crack-filling material in both spectra are similar to those shown in Figure 2-5 for the sample coating. The results for the two locations, reported in Table 2-3, reveal that serpentine is the material filling the crack. As expected, the serpentine is rich in silicon and magnesium, with a low aluminum concentration. There is also significant concentration of iron and nickel, higher than that in the external surface, suggesting there may be a grunierite component to the serpentine.

Table 2-3. Scanning Electron Microscope–Energy-Dispersive X-Ray Analyses of Crack-Filling Serpentine in Josephinite Subsample JS–JB1–S1

Element	Location 1 {9 mm [0.4 in] from Outer Surface}		Location 2 {5 mm [0.2 in] from Outer Surface}	
	Weight Percent	Atomic Percent	Weight Percent	Atomic Percent
Magnesium	35.78	43.90	34.56	42.63
Aluminum	2.20	2.43	0.82	0.91
Silicon	40.30	42.83	41.71	44.53
Sulfur	1.04	0.96	Not determined	Not determined
Calcium	0.28	0.21	Not determined	Not determined
Manganese	Not determined	Not determined	0.18	0.10
Iron	7.77	4.16	8.32	4.47
Nickel	12.23	6.22	14.41	7.36
Copper	0.40	0.19	Not determined	Not determined

In addition to the crack, there are many areas distributed in the JS–JB1 sample in which voids and vugs are abundant, as shown by the scanning electron microscope image in Figure 2-9. Energy-dispersive x-ray analyses show that these voids and vugs are also filled with serpentine as indicated by the typical values of magnesium and silicon found, together with smaller concentrations of nickel, iron, aluminum, and calcium, as listed in Table 2-4. At lower magnification, there also appears to be a serpentine-rich zone as a band at the top of the JS–JB1 sample (Figure 2-1) that extends from the outer surface approximately 5–10 mm [0.2–0.4 in] into the sample.

Table 2-4. Representative Scanning Electron Microscope–Energy-Dispersive X-Ray Analyses of Voids and Vugs in the Josephinite Subsample JS–JB1–S1

Element	Weight Percent	Atomic Percent
Magnesium	39.28	45.25
Aluminum	0.56	4.01
Silicon	48.80	48.65
Calcium	0.14	0.10
Iron	2.97	1.49
Nickel	8.25	3.94

Nevertheless, the metallic phase clearly predominates in the volume of the sample, as illustrated in Figure 2-9, in clear agreement with a wet-chemical analysis of a small sample {3 g [10.6 oz]} taken from the center of the original sample JS–JB1 (Table 2-5). Although the composition given in Table 2-5 may not be fully representative of the whole sample as a result of its apparent heterogeneity, it is a clear indication of the predominance of the nickel-iron alloy.

The composition of the metallic phase in which nickel and iron predominate is given for the two locations along the crack in Table 2-6. The values reported for each location represent an average of six measurements along a line perpendicular to the crack. Three positions at each side of the crack were analyzed for a total length of 600 μm [24 mils]. In addition to small amounts of silicon and copper, trace amounts of magnesium were detected in only a few positions, presumably as a result of the close presence of serpentine-filling voids. The concentrations of nickel and iron are close to the atomic percentages corresponding to stoichiometric Ni_3Fe, even though the nickel content is slightly lower. These concentrations are consistent with those reported in earlier studies (Botto and Morrison, 1976). It is important to note that none of the analyses shows detectable quantities of cobalt, as reported for other samples of josephinite collected from the stream bed of Josephine Creek (Bird, et al., 1979; Bassett, et al., 1980), nor the presence of α-Fe (with less than 5.5 wt% nickel) as a second phase. This body center cubic phase was observed by Bird and Weathers (1975) in some josephinite samples as an assemblage together with the face center cubic γ-Ni-Fe alloy, which is the predominant metallic component of sample JS–JB1.

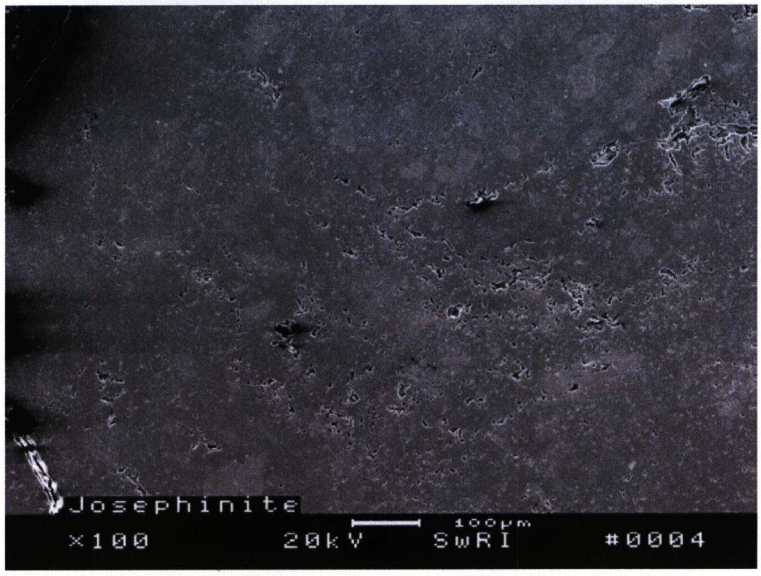

Figure 2-9. Scanning Electron Microscope Image of a Polished Surface of the Josephinite Sample JS–JB1 Exhibiting the Presence of Voids and Vugs Filled with Serpentine Dispersed on a Predominant Metallic Phase (100 µm = 3.9 mils)

Table 2-5. Chemical Composition of Sample at the Center of Josephinite Sample JS–JB1

Composition	Silicon	Aluminum	Arsenic	Carbon	Oxygen	Iron	Nickel
Weight Percent	0.40	<0.01	<0.01	0.03	0.60	21.51	77.26
Atomic Percent	0.81	<0.02	<0.02	0.14	2.14	21.93	74.95

Table 2-6. Scanning Electron Microscope–Energy-Dispersive X-Ray Analysis of Metallic Phase in Josephinite Subsample JS–JB1–S1				
	Location 1 {9 mm [0.4 in] from Outer Surface}		Location 2 {5 mm [0.2 in] from Outer Surface)	
Element	Weight Percent	Atomic Percent	Weight Percent	Atomic Percent
Silicon	0.22 ± 0.05	0.46 ± 0.10	0.59 ± 0.45*	1.2 ± 0.90
Iron	24.18 ± 0.58	25.06 ± 0.60	25.22 ± 0.31	25.96 ± 0.55
Nickel	74.82 ± 0.55	73.77 ± 0.57	73.50 ± 0.75	71.96 ± 1.55
Copper	0.79 ± 0.06	0.72 ± 0.05	0.85 ± 0.75[a]	0.78 ± 0.75
*Detected in only four determinations				

An important feature of the sample JS–JB1 is the presence of another intermetallic, shown in Figure 2-10 as light gray, second-phase particles or inclusions dispersed in the predominant nickel-iron metallic phase, which is the one exhibiting a dark gray appearance. Many black spots associated with serpentine inclusions are also seen. The average values obtained from scanning electron microscope–energy-dispersive x-ray analyses of three different intermetallic inclusions are given in Table 2-7. These inclusions correspond to a nickel-arsenic intermetallic, as noted previously by Bird (2001), in this case with the approximate stoichiometry of Ni_3As_2. Nevertheless, as it can be inferred from the chemical analyses listed in Table 2-5, the proportion of the Ni_3As_2 intermetallic in the JS–JB1 sample is extremely low compared with the nickel-iron alloy phase.

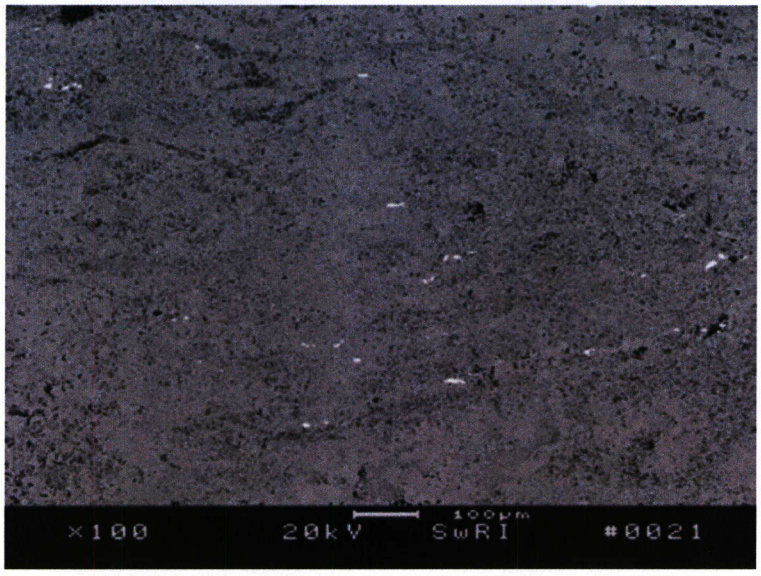

Figure 2-10. Scanning Electron Microscope Image of a Polished Surface of the Josephinite Sample JS–JB1 Exhibiting the Presence of Ni_3As_2 Intermetallic Phase (Light Gray) Dispersed in a Predominant Ni_3Fe Phase (Dark Gray). Voids Filled with Serpentine (Black Spots) are Noticeable. (100 µm = 3.9 mils)

Table 2-7. Scanning Electron Microscope–Energy-Dispersive X-Ray Analyses of Second Intermetallic Phase in Josephinite Sample JS–JB1

Element	Weight Percent	Atomic Percent
Aluminum	0.90 ± 0.04*	2.12 ± 0.09
Silicon	0.30 ± 0.29	0.68 ± 0.64
Iron	1.83 ± 0.63	2.09 ± 0.72
Nickel	55.65 ± 1.91	60.4 ± 1.95
Arsenic	41.63 ± 4.14	35.41 ± 1.87

*Detected in only two of the three inclusions

3 ELECTROCHEMICAL BEHAVIOR OF JOSEPHINITE

One objective of this study is to evaluate the electrochemical behavior of josephinite in a typical carbonated groundwater, characterized by a slightly alkaline pH caused by the presence of bicarbonate among other anionic and cationic species. The purpose was to compare the anodic behavior of josephinite with that of a synthetic nickel-iron alloy of the same composition, in terms of the main alloying elements present in josephinite, and establish the environmental conditions leading to passivity in both materials. A more concentrated solution of the same species with a high pH was also used for comparison.

3.1 Effect of Simulated Groundwater on Josephinite

In these studies, a solution was used in which the predominant anions are those present in J–13 Well water and in the pore water found in the unsaturated zone in the vicinity of Yucca Mountain (Table 2-1). The composition of the solution, designated as simulated groundwater, is given in Table 3-1. The solution was simplified with respect to that used in the long-term corrosion test facility at the Lawrence Livermore National Laboratory (CRWMS M&O, 2000a) by eliminating SiO_2 and using only Na^+ and K^+ as metal cations. More importantly, to be comparable with that of J–13 Well water, the concentration of the various species is approximately one order of magnitude lower than that used in the long-term corrosion test facility. The pH of the simulated groundwater solution was 8.3, and solutions of higher pH were prepared by adjusting the pH with the addition of NaOH. A limited number of tests were conducted in a more concentrated solution, designated as basic saturated water (CRWMS M&O, 2000a), in which HCO_3^- was excluded because the pH was adjusted to 13.0 by the addition of NaOH. The composition of this solution, derived from evaporation experiments from a relatively concentrated solution of the predominant species present in groundwater (CRWMS M&O, 2000a), is also given in Table 3-1.

Table 3-1. Chemical Composition of Simulated Groundwater and Basic Saturated Water Used Used to Study the Anodic Behavior of Josephinite

	Simulated Groundwater		Basic Saturated Water	
Ionic Species	mg/L	mM	mg/L	mM
Na^+	36.0	1.57	109.7	4.77
K^+	3.4	0.09	67.7	1.73
HCO_3^-	70.0	1.14	—	—
Cl^-	6.4	0.18	133.0	3.75
SO_4^{2-}	17.3	0.18	14.4	0.15
NO_3^-	6.4	0.10	141.1	2.28
F^-	1.4	0.07	1.5	0.08

Electrochemical tests were conducted at room temperature {23 °C [73 °F]} in a 1-L Avesta glass cell (Qvarfort, 1988). The cell contains a port with a sealing gasket that allows the positioning of a flat sample and exposure to the solution of a well-defined area of approximately 1 cm^2 [0.15 in^2]. The sealing gasket of the Avesta cell is flooded with the test solution during the electrochemical measurements to avoid the initiation of crevice corrosion at the specimen-gasket interface. Prior to the start of a test, the cut face of the josephinite sample JS–JB1 was mechanically polished to a 600-grit finish, cleaned ultrasonically in a detergent, rinsed in deionized water, ultrasonically cleaned in acetone, dried, and mounted into the cell. A platinum counter electrode was emplaced in the cell, and a saturated calomel electrode, connected to the solution through a Luggin probe with a porous silica tip, was used as a reference electrode. Deaeration was accomplished by purging the solution with high-purity nitrogen (99.999 percent) for at least one hour prior to the start of the test and continued throughout the test. The pH of the solutions was measured before and after each test.

The anodic behavior was evaluated using cyclic potentiodynamic polarization tests according to ASTM Standard G61 (ASTM International, 1999), which involves scanning the potential applied to the specimen from cathodic to anodic potentials and simultaneous monitoring of the current response. The cyclic potentiodynamic polarization scans were conducted at a scan rate of 0.167 mV/s, starting from a cathodic potential 200 mV lower than the open circuit potential, and the direction of the scan was reversed at a current density of 1 mA/cm^2 [9.3×10^2 mA/ft^2] or at 1.0 V_{SCE} when that current density was not reached. The reverse scan was terminated at cathodic potentials, usually 200 mV lower than the initial open circuit potential. The open circuit potential or corrosion potential in the deaerated solutions was measured just before polarization was started. At the conclusion of each test, the specimens were examined with an optical microscope.

A cyclic potentiodynamic polarization curve for the josephinite sample JS–JB1 in simulated groundwater at room temperature {23 °C [73 °F]} and pH 8.3 is shown in Figure 3-1. It is apparent that josephinite in this solution exhibits an active anodic behavior. After scanning the potential from cathodic to anodic potentials passing through the open circuit potential (cathodic currents are indicated with dashed lines in all figures), the anodic current density in the forward scan increases monotonically with potential following an almost active Tafelian dependence (i.e., logarithm of the current density tends to be directly proportional to the applied potential). Even though a minor, positive hysteresis loop is noticeable in the reverse potentiodynamic scan, the current densities in both the forward and reverse scans are similar. In agreement with this observation, the josephinite surface did not show any signs of localized corrosion after being examined in the optical microscope.

The effect of solution pH on the anodic behavior of josephinite can be observed in the four cyclic potentiodynamic polarization curves plotted in Figure 3-2. With increasing pH, a range of passivity (i.e., low anodic current density that tends to be independent of the applied potential) became apparent in the forward potential scan. In addition, at pH levels ranging from 10.0 to 11.9, a noticeable positive hysteresis loop is observed on the reverse potential scan in Figure 3.2(a through c). The hysteresis loop is clearly related to the occurrence of localized corrosion in the form of pits confirmed by optical examination after the tests. During the forward

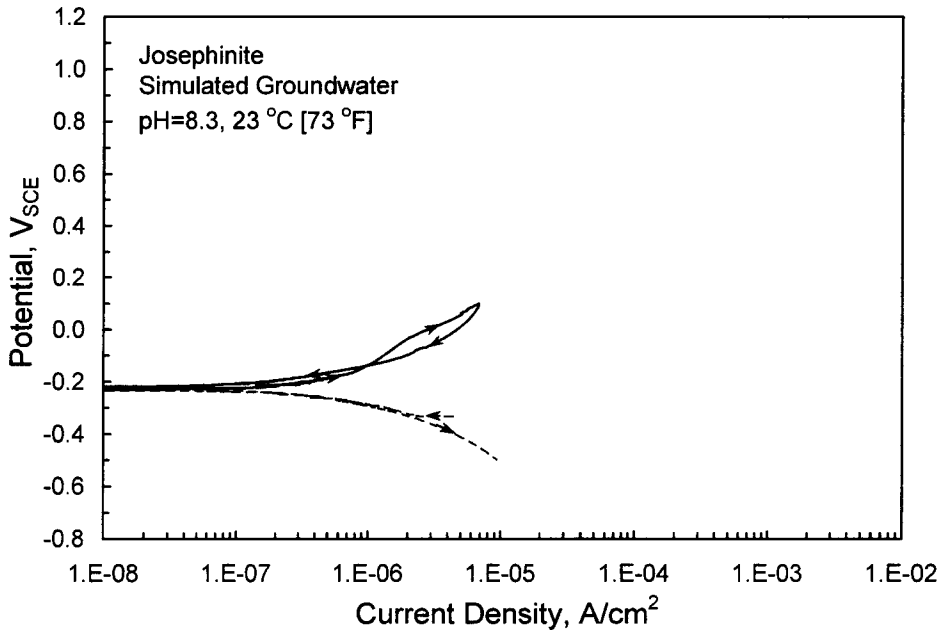

Figure 3-1. Cyclic Potentiodynamic Polarization Curve of Josephinite in Simulated Groundwater (pH 8.3) at Room Temperature Using a Potential Scan Rate of 0.167 mV/s

potential scan, the current density increased abruptly at a certain critical value, the pitting initiation potential (E_p), indicating the initiation and growth of pits on the josephinite sample. After the pits are grown, they are repassivated during the reverse potential scan. It can be noted in Figure 3.2(a through c) the repassivation potential (E_{rp}) (i.e., the potential value at which the current density decreases below the passive current density) is close to the value of the open circuit potential. At pH 12.8, however, the abrupt current increase observed at potentials more than 0.5 V_{SCE} in Figure 3-2(d) did not correspond to the occurrence of localized corrosion. At this pH, localized corrosion is inhibited, and the anodic current density increased only because of the evolution of oxygen resulting from the electrochemical decomposition of water. The hysteresis loop became negative on reversing the potential because passivity is preserved, as reflected in the low values of the passive current density in the reverse scan. It also can be noticed in Figure 3-2(d) that a cathodic loop exists in the reverse scan at potentials just below the onset of the oxygen evolution reaction, probably related to the reduction of a higher oxidation state nickel oxide formed at high potentials during the forward scan. The current in the passive range is higher at pH 12.8 than at lower pH levels, probably reflecting the increasing solubility of nickel oxide with increasing pH that becomes significant at pH levels above 12 (Pourbaix, 1974). The increase in the passive current density with increasing pH of more than 9.0 has been reported for pure nickel (Heusler, 1978).

It is important to note that the trend in the anodic behavior of josephinite as a function of pH, as shown in Figures 3-1 and 3-2, is related to the relative concentration of aggressive and inhibiting anions in solution. It can be concluded from these figures that josephinite exhibits a passive behavior only in solutions of pH equal to and higher than 10.0. At lower pHs levels,

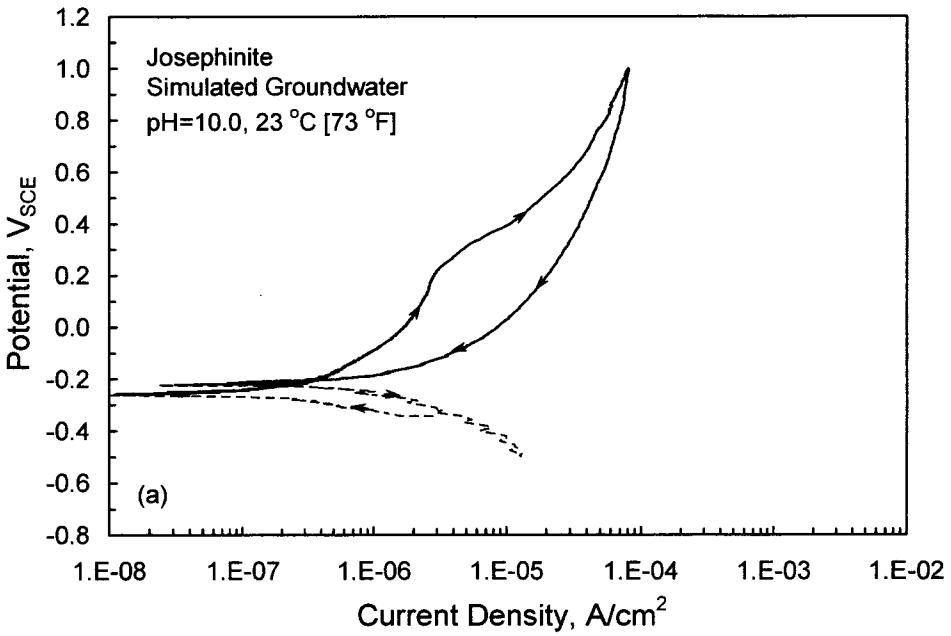

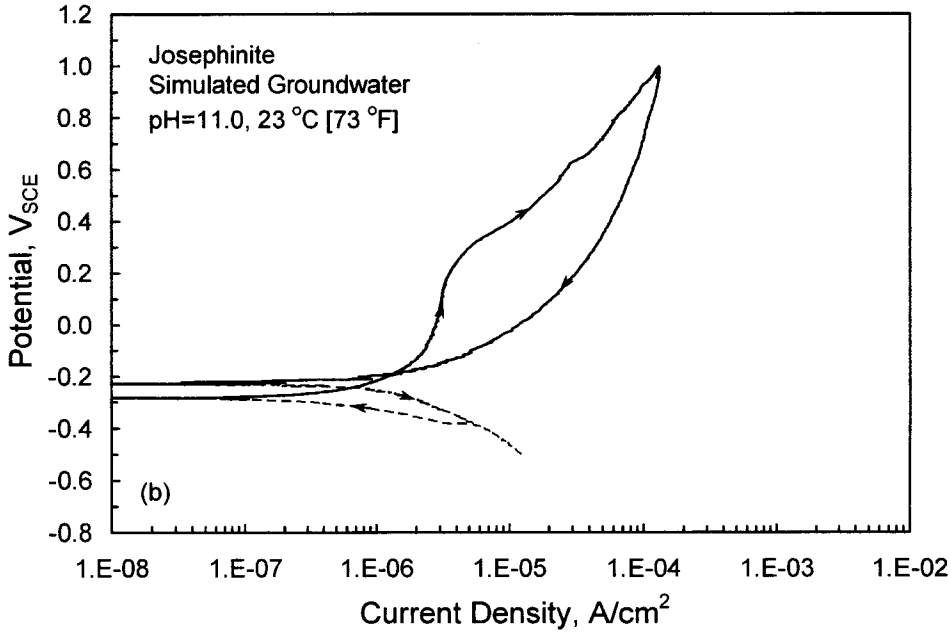

Figure 3-2. Effect of pH on the Cyclic Potentiodynamic Polarization Curves of Josephinite in Simulated Groundwater at Room Temperature Using a Potential Scan Rate of 0.167 mV/s at (a) pH 10.0, (b) pH 11.0, (c) pH 11.9, and (d) pH 12.8

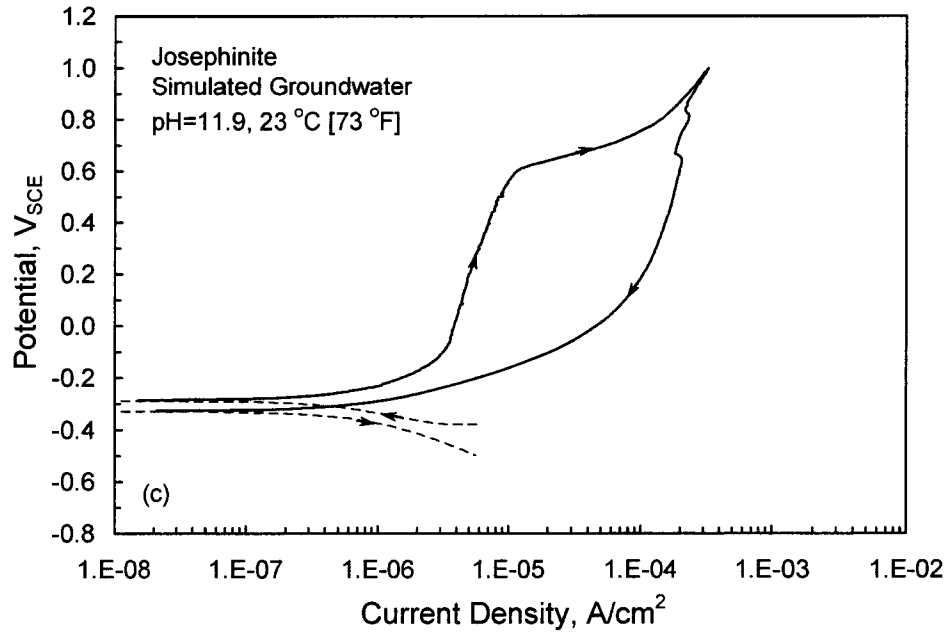

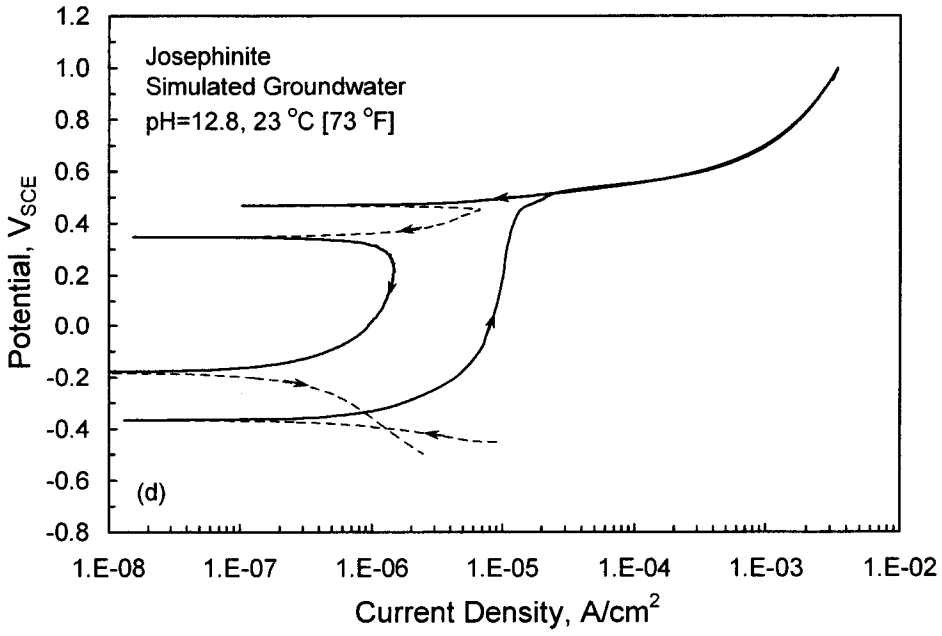

Figure 3-2. Effect of pH on the Cyclic Potentiodynamic Polarization Curves of Josephinite in Simulated Groundwater at Room Temperature Using a Potential Scan Rate of 0.167 mV/s at (a) pH 10.0, (b) pH 11.0, (c) pH 11.9, and (d) pH 12.8 (continued)

active dissolution occurs during anodic polarization. The type of anodic behavior is clearly related to the concentration of the OH^- ion in solution, and it appears that concentrations of at least 10^{-4} molar are required to attain passivity in simulated groundwater. If a passive film is kinetically stable at these high pH levels, the relative concentration of aggressive anions to inhibiting anions would determine the possibility of film breakdown and initiation and growth of pits as the predominant form of localized corrosion. After examining the composition of the simulated groundwater (Table 3-1), it can be concluded that SO_4^{2-}, NO_3^-, and HCO_3^- are potential inhibitors and Cl^- and, in less proportion, F^- are aggressive anions. However, for a given concentration of these species as provided in Table 3-1, the OH^- ion is the main inhibiting species. This observation arises by examining Figure 3-2(a through c), in which it is seen that at pH 10.0 and 11.0, the OH^- to Cl^- molar concentration ratio is not sufficiently high to modify E_p, which is approximately 0.3 V_{SCE}. At pH 11.9, however, the OH^- to Cl^- molar concentration ratio is such that E_p increased to approximately 0.6 V_{SCE}. Finally, as shown in Figure 3-2(d), pitting corrosion is fully inhibited at pH 12.8 by the high OH^- to Cl^- molar concentration ratio in the test solution.

To explore even further the anodic behavior of josephinite, a cyclic potentiodynamic polarization curve was obtained in basic saturated water with a pH of 13.1. As shown in Figure 3-3, josephinite exhibited a passive behavior in this solution. As noted in the simulated groundwater at the same pH, the current density in the passive range is relatively high but almost identical to that in simulated groundwater for the same range. Contrary to the response shown in Figure 3-2(d), passivity breakdown followed by pit initiation and growth occurred during the forward scan when the potential reached a value of approximately 0.1 V_{SCE}. A

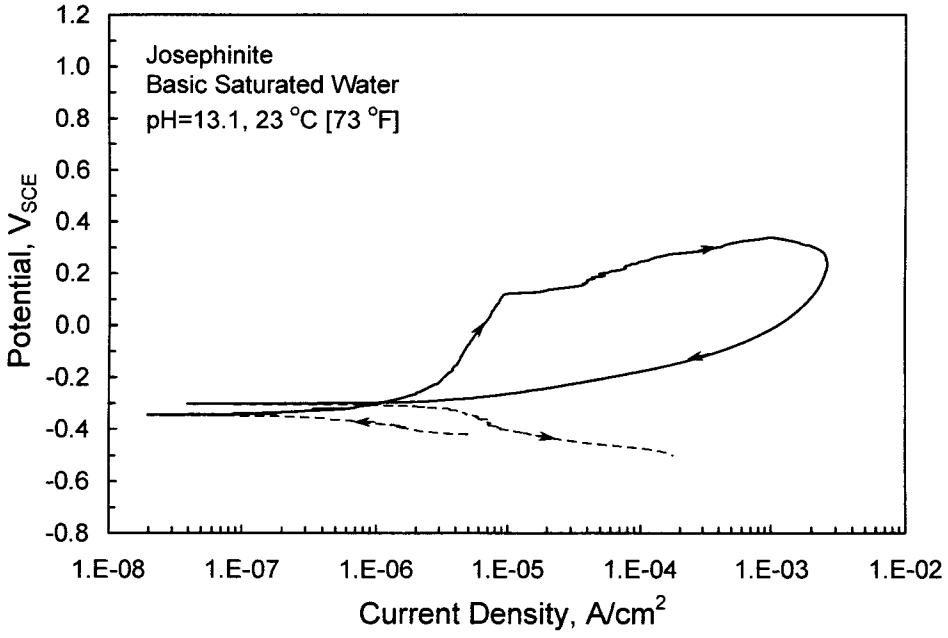

Figure 3-3. Cyclic Potentiodynamic Polarization Curve of Josephinite in Basic Saturated Water (pH 13.1) at Room Temperature Using a Potential Scan Rate of 0.167 mV/s

noticeable positive hysteresis loop is observed in the reverse potential scan, confirming the occurrence of localized corrosion despite the high pH of the solution. Undoubtedly, the OH^- to Cl^- molar concentration ratio in this solution is not sufficiently high to prevent the nucleation and growth of pits during anodic polarization .

3.2 Comparison with Cast Ni_3Fe Alloy

A heat of synthetic Ni_3Fe alloy was prepared by Haynes International, Kokomo, Indiana, using vacuum-induction melting. The chemical composition of the heat, designated as EN 6502-3-981, is given in Table 3-2. The typical microstructure of the cast alloy in two locations is shown in Figure 3-4, in which it is clearly seen that large, elongated grains predominate. It should be noted the ingot exhibited a large number of voids, presumably produced during the solidification processes, however, the material was considered adequate for the present study. Portions of the ingot with the lowest density of voids were selected for machining the specimens in the form of rectangular coupons of approximately 5.0 cm [2 in] in length, 2.5 cm [1 in] in width, and 0.64 cm [0.25 in] in thickness.

Table 3-2. Chemical Composition in Weight Percent of Cast Ni_3Fe Alloy, Heat EN 6502-3-981

Ni*	Fe	Si	P	Cr	Mg	Mn	S	Mo	Pb	C	Cu	Ti
76.34	23.44	<0.01	0.001	<0.01	0.001	<0.01	0.001	0.01	0.001	0.005	<0.01	<0.01

*Notes: Ni—nickel; Fe—iron; Si—silicon; P—phosphorus; Cr—chromium; Mg—magnesium; Mn—manganese; S—sulfur; Mo—molybdenum; Pb—lead; C—carbon; Cu—copper; Ti—titanium

Electrochemical tests, similarly to those performed with josephinite, were conducted on the cast Ni_3Fe alloy samples. The main difference was the use of a 1-L [0.26-gal] glass cell in which the solution can be heated to 95 °C [203 °F] using an external heating tape. An Incoloy 825 wire was spot welded to the coupons to make the electrical connection. The area exposed to the solution, approximately 1 cm^2 [0.16 in^2], was defined by using Micro-Stop as an insulator coating that also covered the spot welded area and the lead wire.

A cyclic potentiodynamic polarization curve for the cast Ni_3Fe alloy in simulated groundwater at pH 8.3 and 23 °C [73 °F] is shown in Figure 3-5. It is apparent that, contrary to the active anodic behavior of josephinite in this solution, the Ni_3Fe alloy exhibits a passive behavior. After scanning the potential from cathodic to anodic potentials, passing through the open circuit potential, the anodic current density became almost independent of potential, indicating that passivity occurred. At a potential of approximately 0.2 V_{SCE}, the current density increased abruptly, indicating the initiation and growth of pits on the sample. A pronounced positive hysteresis loop also revealed the occurrence of localized corrosion, which was confirmed by the observation of pits in the posttest examination using an optical microscope.

The effect of solution pH on the anodic behavior of the cast Ni_3Fe alloy in simulated groundwater at 23 °C [73 °F] is presented in the four cyclic potentiodynamic polarization curves plotted in Figure 3-6. It is evident that passive behavior occurred at all the pH levels ranging

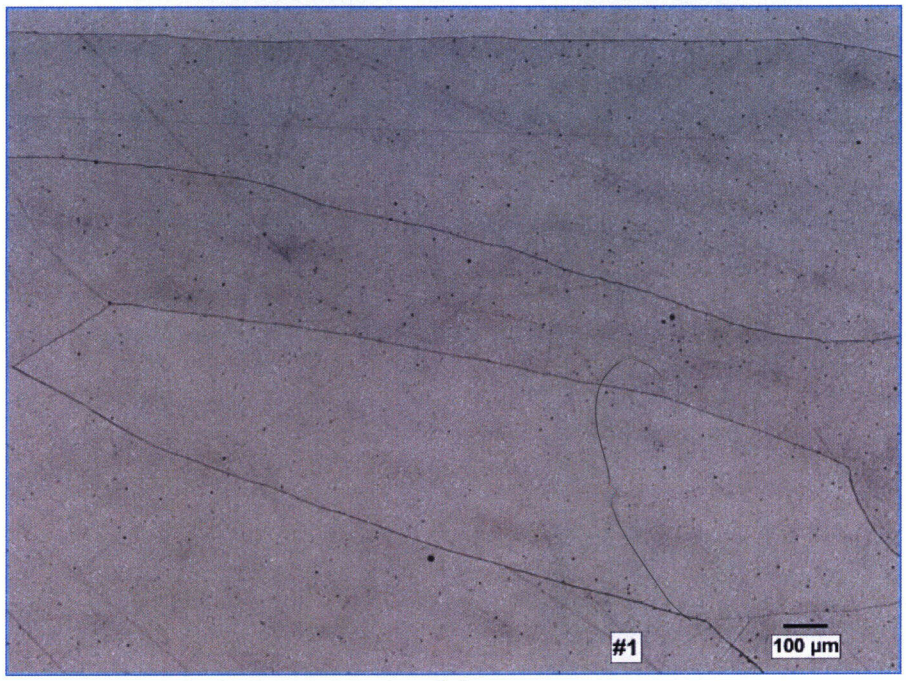

(a)

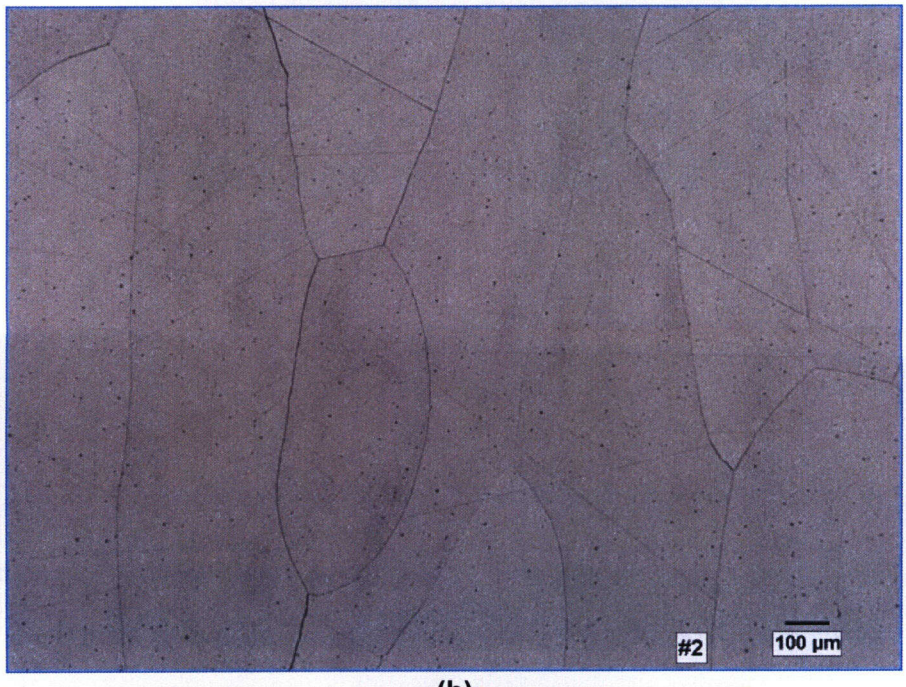

(b)

Figure 3-4. Optical Micrograph Showing the Microstructure of the Cast Ni_3Fe Alloy in Two Locations (100 µm = 3.9 mils)

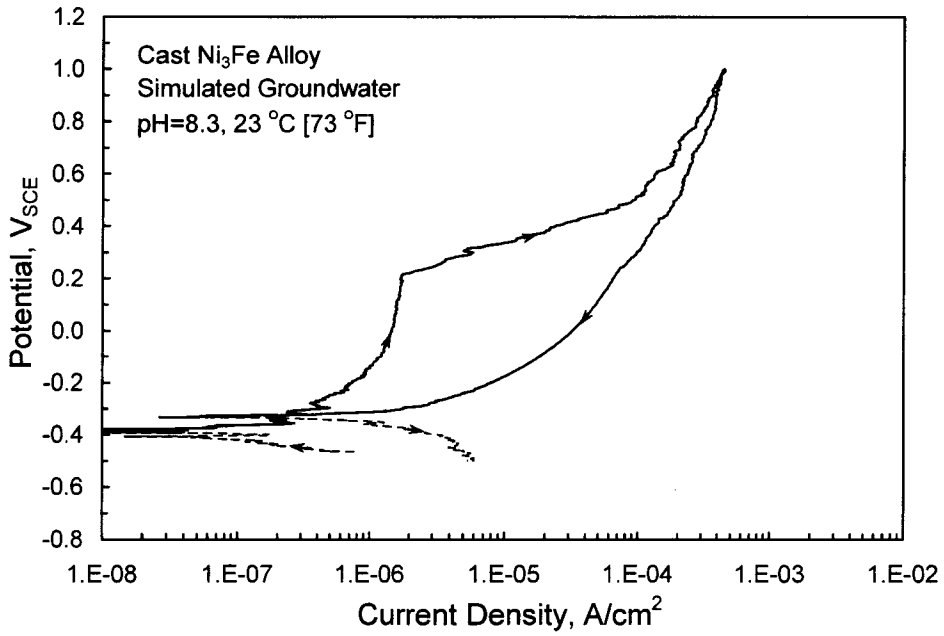

Figure 3-5. Cyclic Potentiodynamic Polarization Curve of the Cast Ni_3Fe Alloy in Simulated Groundwater (pH 8.3) at Room Temperature Using a Potential Scan Rate of 0.167 mV/s

from 10.0 to 12.8. At pH 10.0, E_p increased to 0.7 V_{SCE}, as shown in Figure 3-6(a), a value 500 mV higher than that observed at pH 8.3 (Figure 3-5). It is also 500 mV higher than that measured on josephinite at the same pH [Figure 3-2(a)]. This observation indicates that the OH^- ions are more effective inhibitors of localized corrosion for the cast Ni_3Fe alloy than for josephinite. At even higher pH levels, as shown in Figure 3-6(b through d), localized corrosion is fully inhibited by the OH^- ions, as revealed by the negative hysteresis observed in all these cyclic potentiodynamic polarization curves. The sharp fluctuations of current density observed in the reverse potential scans of these curves, in which even cathodic currents can be noted, are presumably related to electrochemical noise, became more noticeable at these low current densities {$<1 \times 10^{-7}$ A/cm^2 [9.3×10^{-5} A/ft^2]} rather than to stable passivity breakdown events. This interpretation is supported by the low values of the passive current density observed in the forward scans {$<1 \times 10^{-6}$ A/cm^2 [9.3×10^{-4} A/ft^2]} in Figure 3-6(b and c) and the lack of any significant current fluctuations. At pH 12.8, as shown in Figure 3-6(d), the current density is not completely independent of potential during the passive range, even though it is lower than 4×10^{-6} A/cm^2 [3.7×10^{-3} A/ft^2] at the potential corresponding to the onset of the oxygen evolution reaction. In the case of josephinite, it appears that at this high pH, the passive current is higher than that at lower pH levels and increases with the potential in the passive range, as reported for pure nickel in dilute LiOH solutions (Macdonald and Owen, 1976).

The effect of temperature on the anodic behavior of the cast Ni_3Fe alloy in simulated groundwater is presented in the four cyclic potentiodynamic polarization curves plotted in Figure 3-7. The cyclic potentiodynamic polarization curve in Figure 3-7(a) can be compared

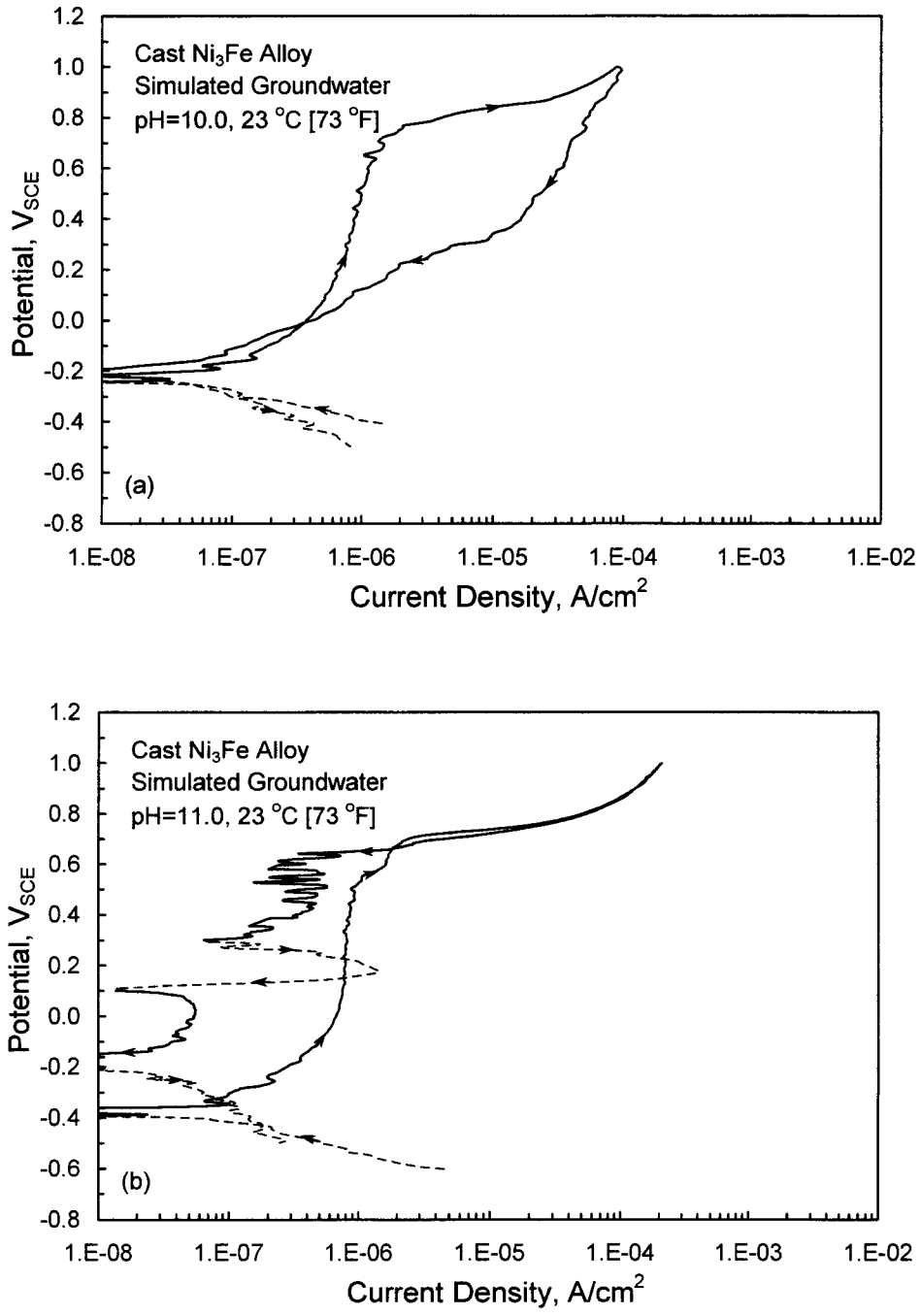

Figure 3-6. Effect of pH on the Cyclic Potentiodynamic Polarization Curves of the Cast Ni_3Fe Alloy in Simulated Groundwater at Room Temperature Using a Potential Scan Rate of 0.167 mV/s at (a) pH 10.0, (b) pH 11.0, (c) pH 12.0, and (d) pH 12.8

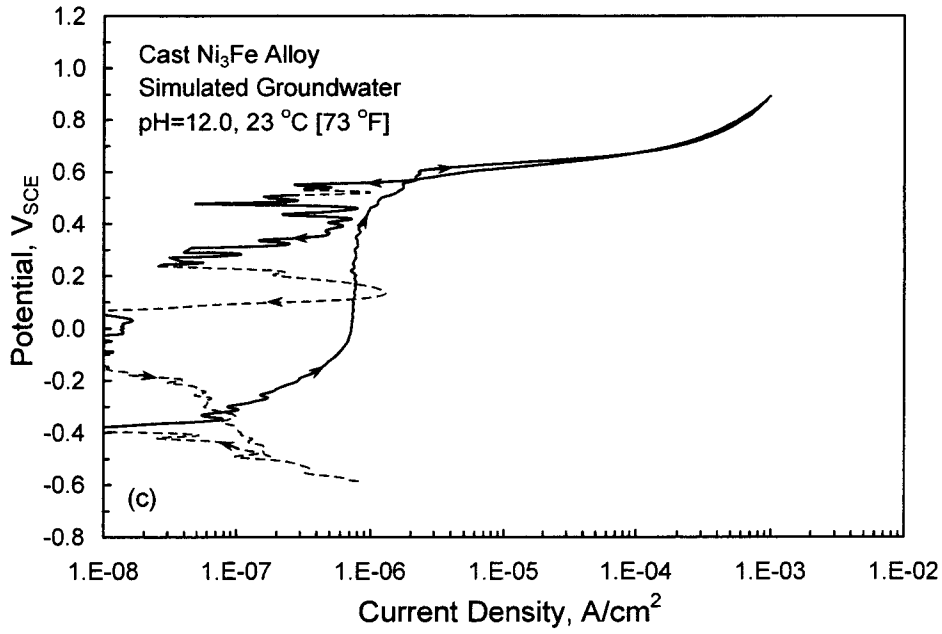

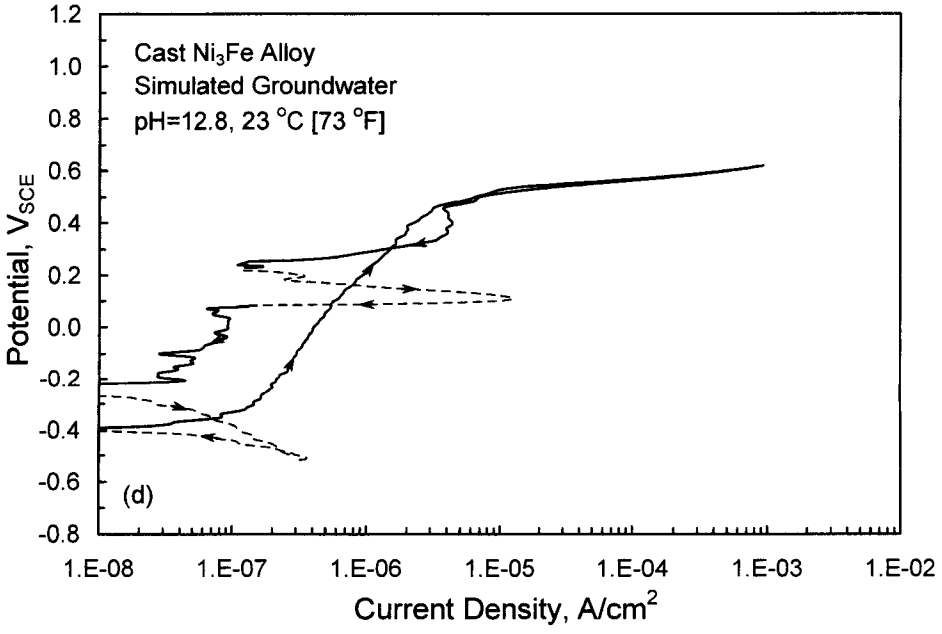

Figure 3-6. Effect of pH on the Cyclic Potentiodynamic Polarization Curves of the Cast Ni_3Fe Alloy in Simulated Groundwater at Room Temperature Using a Potential Scan Rate of 0.167 mV/s at (a) pH 10.0, (b) pH 11.0, (c) pH 12.0, and (d) pH 12.8 (continued)

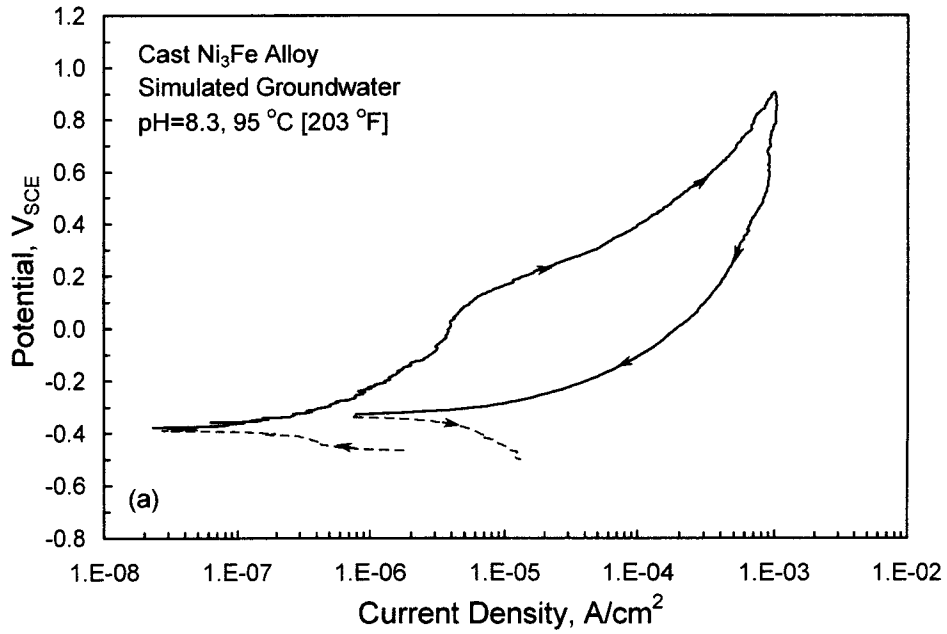

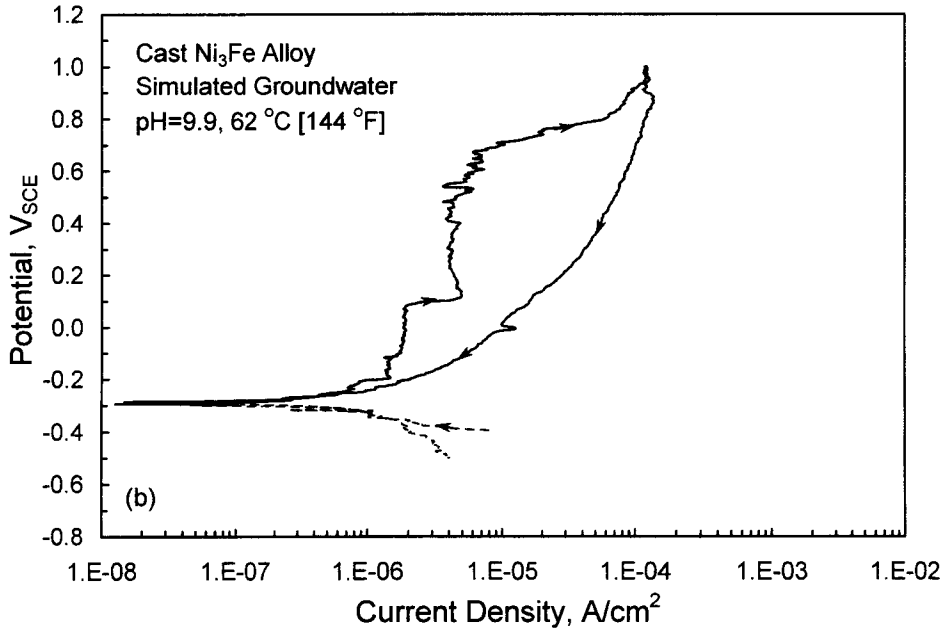

Figure 3-7. Effect of Temperature on the Cyclic Potentiodynamic Polarization Curves of the Cast Ni_3Fe Alloy in Simulated Groundwater Using a Potential Scan Rate of 0.167 mV/s at (a) pH 8.3 and 95 °C [203 °F], (b) pH 9.9 and 62 °C [144 °F], (c) pH 10.0 and 79 °C [174 °F], and (d) pH 10.0 and 92 °C [198 °F]

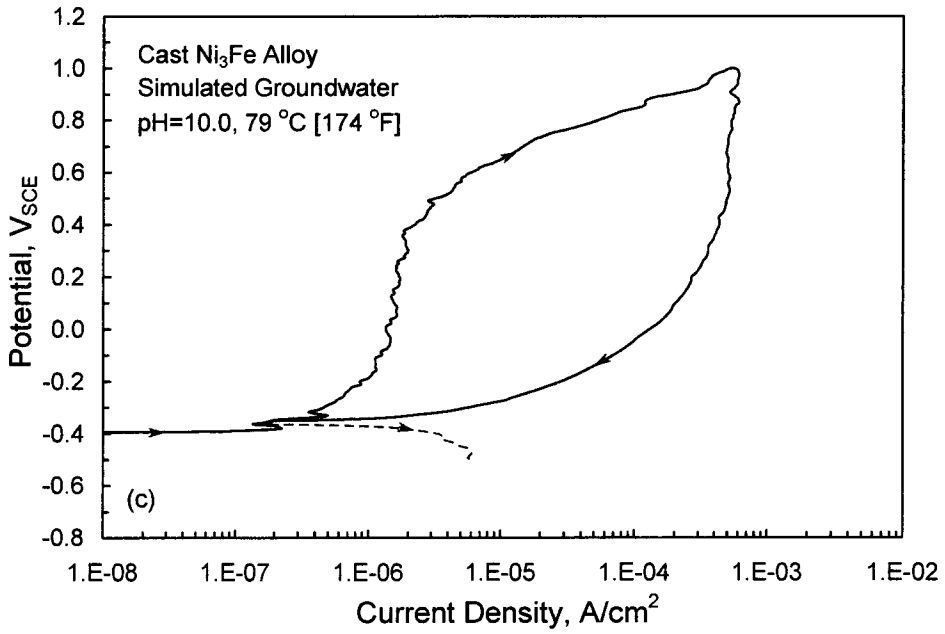

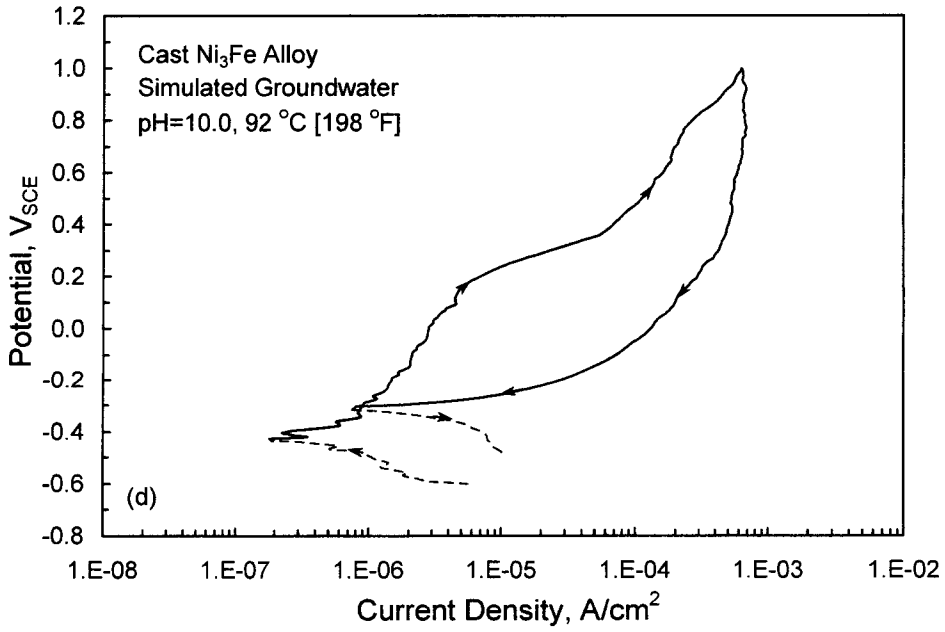

Figure 3-7. Effect of Temperature on the Cyclic Potentiodynamic Polarization Curves of the Cast Ni_3Fe Alloy in Simulated Groundwater Using a Potential Scan Rate of 0.167 mV/s at (a) pH 8.3 and 95 °C [203 °F], (b) pH 9.9 and 62 °C [144 °F], (c) pH 10.0 and 79 °C [174 °F], and (d) pH 10.0 and 92 °C [198 °F] (continued)

with that in Figure 3-5 because both curves were obtained at pH 8.3. It is apparent that at 95 °C [203 °F], the passive current density is higher than that at 23 °C [73 °F] and not so independent of potential. In addition, E_p decreased by approximately 100 mV, but the increase in the current density is not so abrupt and is probably related to the higher current density prevailing within the passive range at the higher temperature. Figure 3-7(b through d) shows the effect of increasing temperature on the anodic behavior of the cast Ni_3Fe alloy at pH 10.0. There is no noticeable effect of increasing temperature on the value of the passive current density to 79 °C [174 °F] [Figures 3-7(b and c)], even though more current fluctuations are observed at 62 and 79 °C [144 and 174 °F], as compared with the cyclic potentiodynamic polarization curve at 23 °C [73 °F] [Figure 3-6(a)]. At 92 °C [198 °F], however, the current density in the passive range increases with the potential, similar to that observed at approximately the same temperature in the pH 8.3 solution, as seen by comparing Figure 3-7(d) with Figure 3-7(a). The increase in temperature also affects the value of E_p as noted previously for pH 8.3 solution. By comparing the cyclic potentiodynamic polarization curves in Figure 3-6(a) with those in Figure 3-7(b through d), it is seen that E_p remained equal to 0.7 V_{SCE} by increasing the temperature from 23 to 62 °C [73 to 144 °F]. At higher temperatures, however, E_p decreased to 0.4 V_{SCE} at 79 °C [174 °F] and to 0.2 V_{SCE} at 92 °C [198 °F]. It should be noted that E_{rp} in all these cases is practically equal to −0.3 V_{SCE}, which is the value of the open circuit potential, with the exception of the pH 10.0 solution at room temperature in which E_{rp} is equal to 0.0 V_{SCE}. This value is approximately 200 mV higher than the open circuit potential and corresponds to the solution in which E_p is strongly inhibited by the relatively high OH^- to Cl^- molar concentration ratio.

As with josephinite, a cyclic potentiodynamic polarization curve of the cast Ni_3Fe alloy was obtained in basic saturated water (pH 13.1) at 23 °C. As shown by comparing Figure 3-8 with Figure 3-3, the cast Ni_3Fe alloy exhibits passive behavior characterized by a significantly lower current density than that of josephinite. In addition, the E_p of the cast alloy is approximately 150 mV higher than that of josephinite but E_{rp} is essentially the same, even though the hysteresis appears to be more pronounced with the cast alloy. As noted previously, a noticeable positive hysteresis loop is observed in the reverse potential scan, confirming the occurrence of localized corrosion despite the high pH of the solution. Undoubtedly, the OH^- to Cl^- molar concentration ratio in this solution is not sufficient to prevent the nucleation and growth of pits upon anodic polarization.

3.3 Passivity of Josephinite and Cast Ni_3Fe Alloy

In a separate set of potentiostatic tests, the anodic current density was measured as a function of time at an applied potential in the passive range. As in the cyclic potentiodynamic polarization tests, the solutions were fully deaerated and maintained at room temperature. Specimens of josephinite and the cast Ni_3Fe alloy exposed to solutions of different pH levels were held potentiostatically at 0 V_{SCE} for approximately 10 hours to attain a stable steady-state current density.

Figure 3-9 shows the effect of pH on the potentiostatic current density versus time plots for josephinite in simulated groundwater at 0 V_{SCE}. At pH 12.5, the anodic current density decreased continuously with time until a steady-state value lower than 1.0×10^{-6} A/cm^2

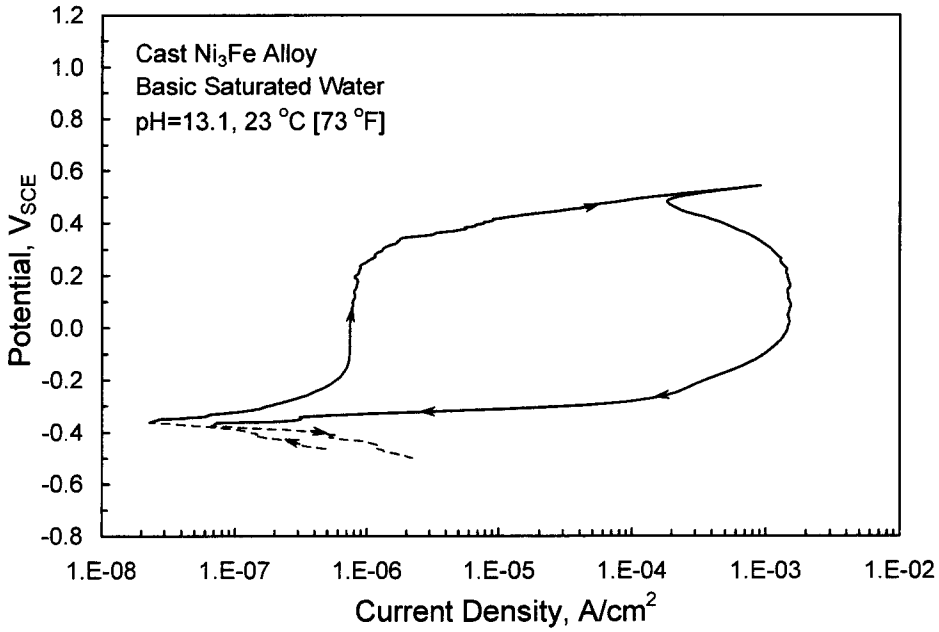

Figure 3-8. Cyclic Potentiodynamic Polarization Curve of the Cast Ni_3Fe Alloy in Basic Saturated Water (pH 13.1) at Room Temperature Using a Potential Scan Rate of 0.167 mV/s

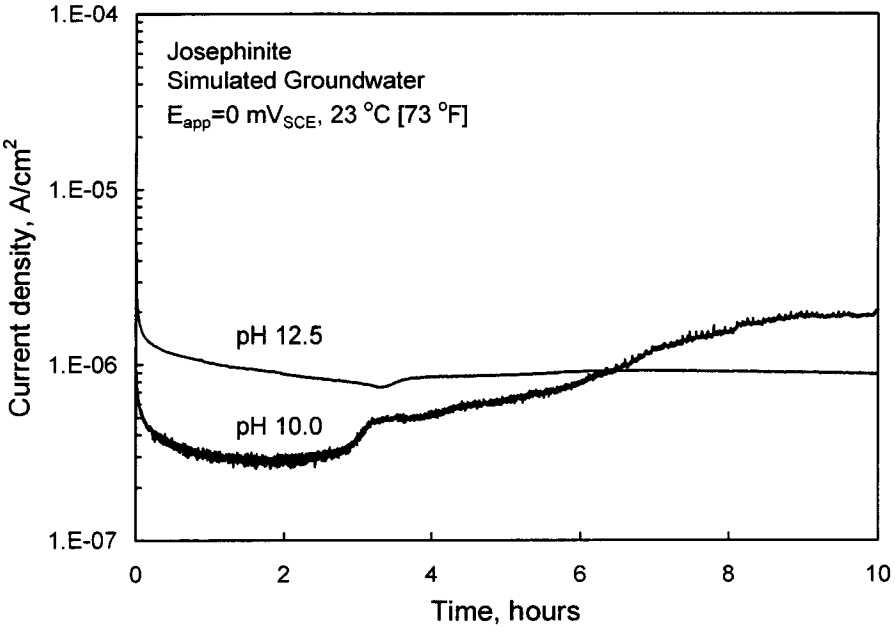

Figure 3-9. Potentiostatic Current Density Versus Time Curves for Josephinite in Simulated Groundwater at Room Temperature with an Applied Potential of 0 V_{SCE} at pH Levels 10.0 and 12.5

[9.3 × 10^{-4} A/ft^2] is attained, indicating that a stable passive film has been formed. At pH 10.0, however, the anodic behavior is clearly different, as shown in Figure 3-9. The current density reached initially an even lower value than that at pH 12.5. After a brief induction period, it began to increase, exhibiting significant fluctuations. This evolution of the current is a clear indication that pitting corrosion occurred at 0 V_{SCE} in simulated groundwater at pH 10.0 as confirmed by optical examination at the end of the experiment. By comparing this result with the cyclic potentiodynamic polarization curve shown in Figure 3-2(a), it appears that pitting corrosion can occur in josephinite at an applied potential 200 mV lower than the E_p measured by potentiodynamic polarization, but obviously higher than the E_{rp} shown in the same cyclic potentiodynamic polarization curve.

For comparison with the anodic behavior of josephinite, Figure 3-10 shows the effect of pH on the passive current density of the cast Ni_3Fe alloy in simulated groundwater at 0 V_{SCE}. In this case, at both pH levels of 12.5 and 10.0, the anodic current density decreased continuously with time, as shown in Figure 3-10, until a steady-state value slightly lower than 1.0 × 10^{-6} A/cm^2 [9.3 × 10^{-4} A/ft^2] was attained after 10 hours, indicating that a stable passive film has been formed. No pitting corrosion was observed on these specimens.

From these results and those presented in Sections 3.1 and 3.2, it can be inferred that josephinite and the cast Ni_3Fe alloy are able to form a stable passive film in simulated groundwaters at room temperature only when the pH is sufficiently alkaline. The transition from an active anodic behavior to passive dissolution seems to occur between pH 8.3 and 10.0

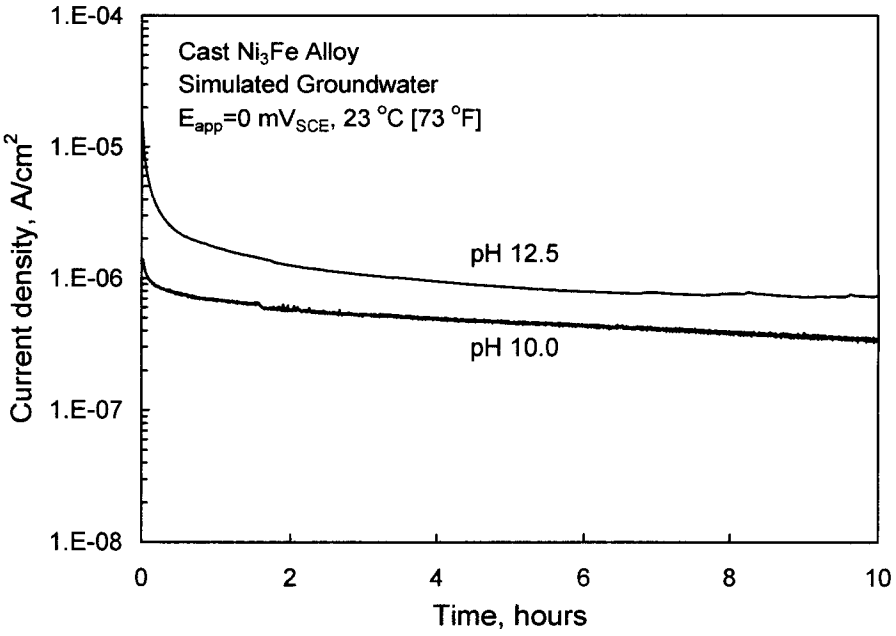

Figure 3-10. Potentiostatic Current Density Versus Time Curves for the Cast Ni_3Fe Alloy in Simulated Groundwater at Room Temperature with an Applied Potential of 0 V_{SCE} at pH Levels 10.0 and 12.5

for josephinite, whereas pH 8.3 seems to be sufficient for the cast Ni_3Fe alloy. At pH levels just above their transition to a passive behavior, josephinite and the cast Ni_3Fe alloy become susceptible to localized corrosion at relatively low anodic potentials. This localized corrosion is a result of passivity breakdown, followed by pit initiation and growth caused by the effect of chloride ions in the environment. Pitting corrosion is inhibited only at a relatively high OH^- to Cl^- molar concentration ratio, and passive behavior predominates for a wide potential range. Despite their close similarity, the cast Ni_3Fe alloy appears to exhibit a slightly different electrochemical response than that of josephinite.

4 CHARACTERIZATION OF JOSEPHINITE PASSIVE LAYERS

The passive surface layers that formed on both josephinite and the cast Ni_3Fe alloy in simulated groundwater were characterized by x-ray photoelectron spectroscopy combined with indepth sputtering. The objective was to determine in a comparative fashion the thickness and chemical composition of the passive films formed on both materials in simulated diluted water of different pH levels after anodic polarization at a potential in the middle of the passive range.

4.1 Passive Layer of Josephinite

Passive films on josephinite were prepared at room temperature {23 ° [73 °F]} by exposing two specimens to simulated groundwater of different pH levels under anodic potentiostatic polarization. For that purpose, sections of josephinite having a distinctive metal appearance were mechanically polished with a diamond paste to a 3-μm [1.18×10^{-4}-in] surface finish. A potential of 0 V_{SCE} was applied for approximately six hours while the current was continuously recorded. A fully passive behavior was obtained at this potential in the pH 12.4 solution in agreement with the polarization curves shown in Figure 3-2 and the current density versus time plot in Figure 3-9. In the pH 9.5 solution, the initiation of pitting corrosion from a passive surface occurred, similar to the results shown in Figure 3-9 for a pH 10.0 solution.

The passive surface layers on the electrochemically treated josephinite samples were analyzed using a Physical Electronics 5400 x-ray photoelectron spectrometer. The Mg Kα anode of the x-ray source was used because the Al Kα source causes an overlap between the Auger transitions of Fe and the Ni 2p peaks. The take-off angle of the photoelectrons was 45 degrees with respect to the sample surface. For each sample, a wide-energy survey was conducted with a pass energy of 89.45 eV to determine surface elemental composition. The survey was followed by a high-resolution scan with a pass energy of 44.75 eV that recorded spectra from four regions corresponding to the core levels of C 1s, O 1s, Fe $2p_{3/2}$, and Ni $2p_{3/2}$. The concentration for element X (C_X) was calculated from the total peak area of the corresponding core-level peak and corrected with the sensitivity factor (Moulder, et al., 1992). The high-resolution spectra were curve fitted to determine the oxidation state of iron and nickel and the chemical-bonding environment for carbon and oxygen. The spectrometer energy scale was calibrated using the 84.0 eV Au $4f_{7/2}$ and 932.67 eV Cu $2p_{3/2}$ peaks with a pass energy of 8.95 eV at 0.05 eV per step. Concentration depth profiles were obtained after argon ion sputtering at 3 keV. The sputtering rate was calibrated by conducting depth profiling through a SiO_2 layer of 1,000 Å [3.93×10^{-6} in] on silicon, giving a rate of 23 Å/min [9.05×10^{-8} in/min].

Figure 4-1 shows the wide-energy survey spectrum of the as-received josephinite sample passivated at pH 9.5. As shown in Figure 4-1, the elements present are nickel, iron, oxygen, carbon, and chlorine. Several spectra were obtained with indepth sputtering. The high-carbon concentration on the as-received surface was caused by atmospheric contamination during transfer of the samples in air.

Concentration depth profiles of the josephinite samples at both pH levels 12.4 and 9.5 are presented in Figure 4-2, where only concentrations of nickel, iron, oxygen, and carbon are provided. The relation between sputtering time and equivalent depth is calculated according to

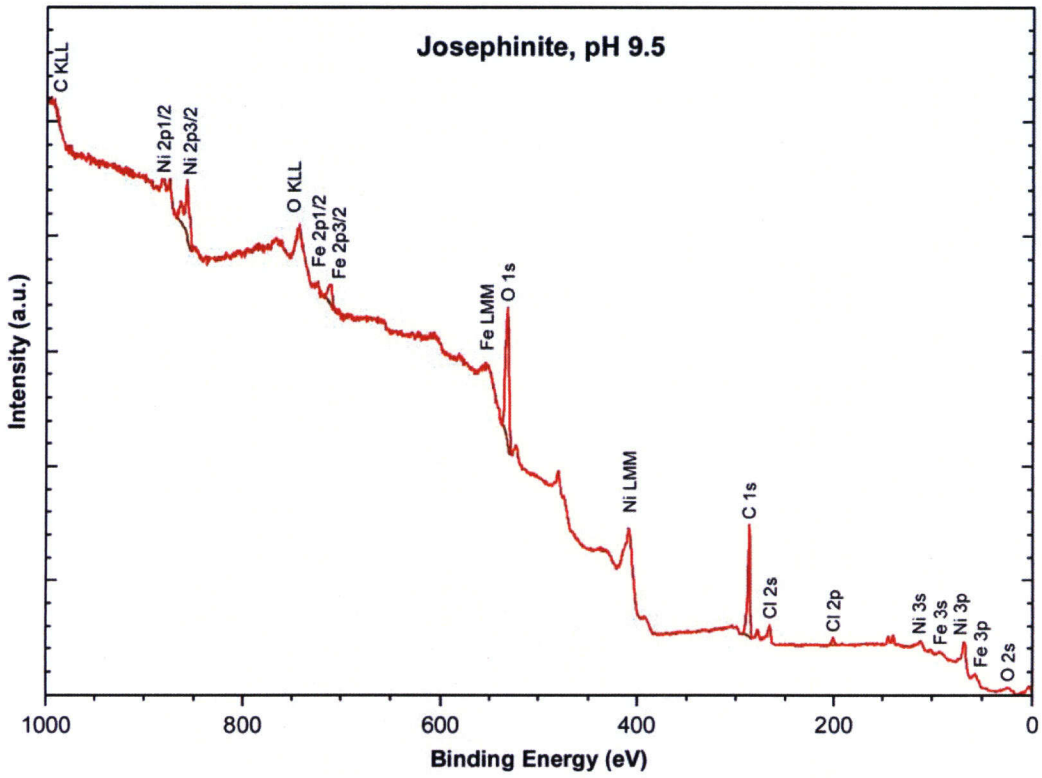

Figure 4-1. Wide-Energy Survey Spectrum of the As-Received Josephinite Passivated in Simulated Groundwater at Room Temperature with an Applied Potential of 0 V_{SCE} at pH 9.5

the sputtering rate obtained from the SiO_2 film. It is clearly seen in Figure 4-2 that three regions can be defined in the concentration depth profiles: the outer contamination layer (I), the inner passive layer (II), and the base material (III). As expected, a high carbon concentration was found in the first surface region. The extent of the region can be determined from the outer surface to the depth where the carbon concentration decreases to approximately 30 atomic percent. The thickness of the outer contamination layer, independent of solution pH, is therefore approximately 4 Å [1.57×10^{-5} mils]. The second surface region represents the passive film, where a mixture of nickel and iron oxides is present. The thickness of the passive film was determined by the depth at which the nickel concentration reached a constant value. It is also noted that within this inner passive layer, the concentration ratio of nickel to iron (C_{Ni}/C_{Fe}) is relatively low, ranging from 2.0 to 3.0, whereas the ratio is approximately 3.4 in the base material. From these criteria, the passive film formed on the josephinite surface after electrochemical treatment at pH 12.4 is approximately 27 Å [4.33×10^{-5} mils], slightly thicker than that formed at pH 9.5. In the josephinite sample anodically treated in the pH 9.5 solution, the presence of chlorine at a concentration of approximately 1.5 atomic percent was detected (Figure 4-1). The presence of chlorine can be

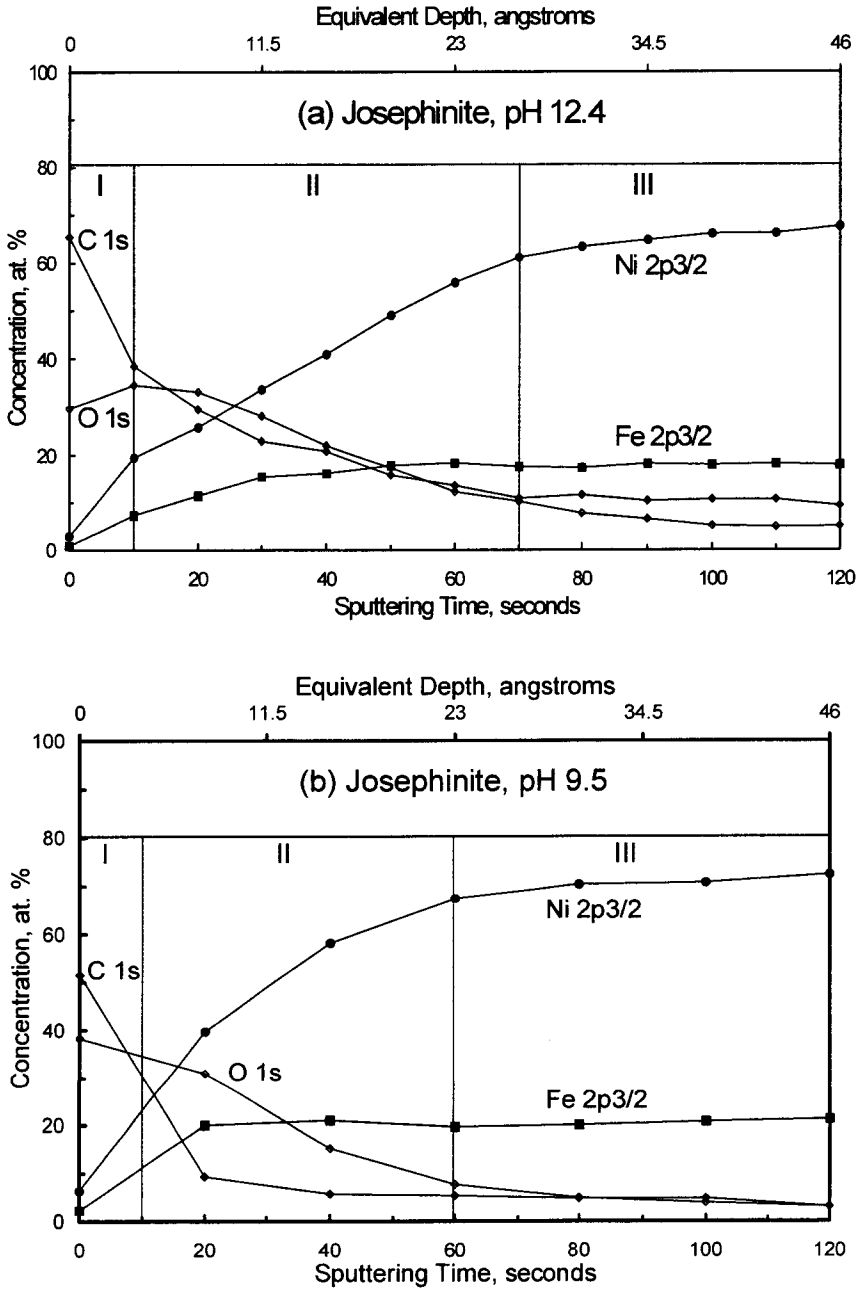

Figure 4-2. Concentration Depth Profiles of Josephinite Passivated in Simulated Groundwater at Room Temperature with an Applied Potential of 0 V_{SCE} at (a) pH 12.4 and (b) pH 9.5. Equivalent Depth Is Relative to the Sputtering Rate of SiO_2 with the Same Conditions.

attributed to surface interactions with the test solution that may have led to a strong adsorption of chloride ions as a precursor to the occurrence of pitting corrosion.

Figure 4-3 shows changes in x-ray photoelectron spectroscopy signals with sputtering time for the two josephinite samples. In the cases of the Fe $2p_{3/2}$ and Ni $2p_{3/2}$ regions, an oxide component with a high binding energy (711.6 eV for iron oxide and 857.6 eV for nickel oxide) and a metallic component with a low binding energy (708.2 eV for metallic iron and 854.0 eV for metallic nickel) can be identified. It should be mentioned that because the differences in binding energy of various oxides and hydroxides of both iron and nickel cannot be accurately resolved, the oxide peaks labeled represent a mixture of oxide and hydroxide species. As shown in Figure 4-3, it is clearly evident in the Fe $2p_{3/2}$ and Ni $2p_{3/2}$ core-level signals that the peak of an oxide component on the as-received surface shifts to a metallic component with increasing sputtering time. For the O 1s region, three distinct peaks are apparent: one at 534.2 eV, corresponding to oxygen in water; a second at 532.3 eV, for OH^- in hydroxide species; and a third at 530.5 eV, corresponding to O^{2-} in iron or nickel oxide. It is shown in Figure 4-3 that water, hydroxide, and oxide species are present on the as-received surfaces, and, after short sputtering times, the peak corresponding to oxide species predominates. The oxide species signals are shown to diminish at the later stage of sputtering when the base material is reached.

The extent of the passive film on josephinite can also be evaluated based on the change of the Fe $2p_{3/2}$ core-level signals with sputtering time. In the case of the electrochemical treatment at pH 12.4, the iron oxide peak at 711.6 eV was observed on the josephinite sample during the initial sputtering period of 60 seconds, whereas it was observed in the sample treated at pH 9.5 only up to the initial 40-second sputtering period The progression of the peak shift in the Fe $2p_{3/2}$ core-level signals observed with indepth sputtering provides an estimate of the passive film thickness, which is comparable to that estimated from the concentration depth profiles.

The contributions of each of the species were extracted by deconvoluting the curve of the Fe $2p_{3/2}$, Ni $2p_{3/2}$, and O 1s core-level signals. Figure 4-4 shows the high-resolution spectrum curve fits of the Fe $2p_{3/2}$, Ni $2p_{3/2}$, and O 1s regions of josephinite passivated at pH 12.4 before and after sputtering for 40 and 120 seconds. Each of the core-level signals was fitted by a linear combination of characteristic peaks of corresponding species. One characteristic peak in the Ni 2p signal that is not identified is the result of multiple splitting of the Ni $2p_{3/2}$ core-level. Although both the Fe $2p_{3/2}$ and Ni $2p_{3/2}$ core-level signals were fitted with a combination of an oxide peak and a metallic peak, the O 1s signal was fitted with three peaks corresponding to water, hydroxide, and oxide species. Hence, a separate contribution of each species could be calculated. The calculated contributions of various species are given in Table 4-1. It is clearly seen in Table 4-1 the contributions of the components used to fit the spectra vary with sputtering time. According to the extent of the three surface regions discussed previously, these three sets of curve fits represent examples within the outer contamination layer, inner passive layer, and base material on the josephinite sample after passivation at pH 12.4 in simulated groundwater. As anticipated from the as-received surface, the contributions of iron and nickel oxides were found to predominate in the outer contamination layer. It is also interesting to note the persistence of significant contributions of iron and nickel oxides after sputtering for 120 seconds down to the base material. The total oxide concentration, however,

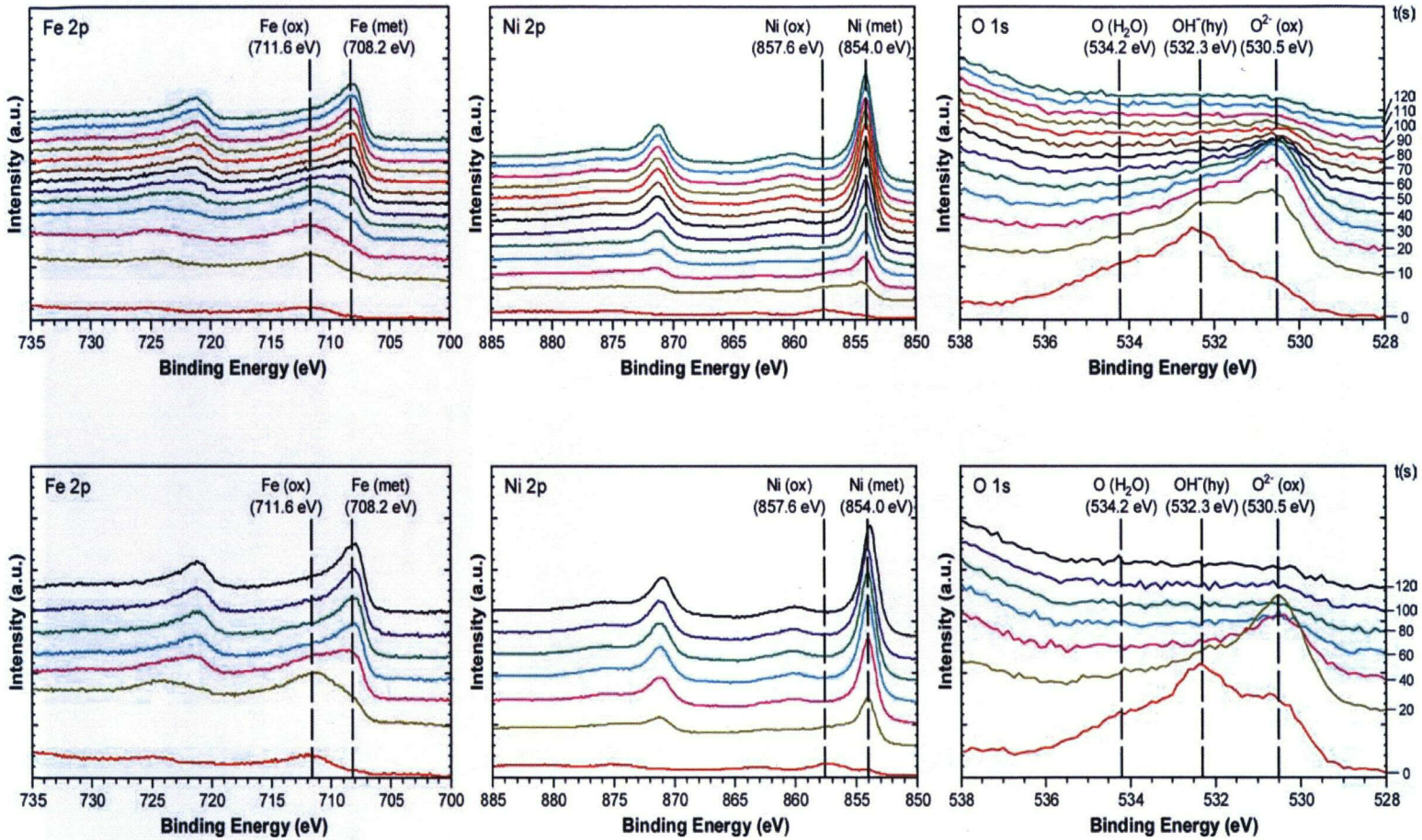

Figure 4-3. Change in Fe 2p, Ni 2p, and O 1s Signals with Sputtering Time of Josephinite Passivated in Simulated Groundwater at Room Temperature with an Applied Potential of 0 V_{SCE} at pH 12.4 (Top Row) and at pH 9.5 (Bottom Row)

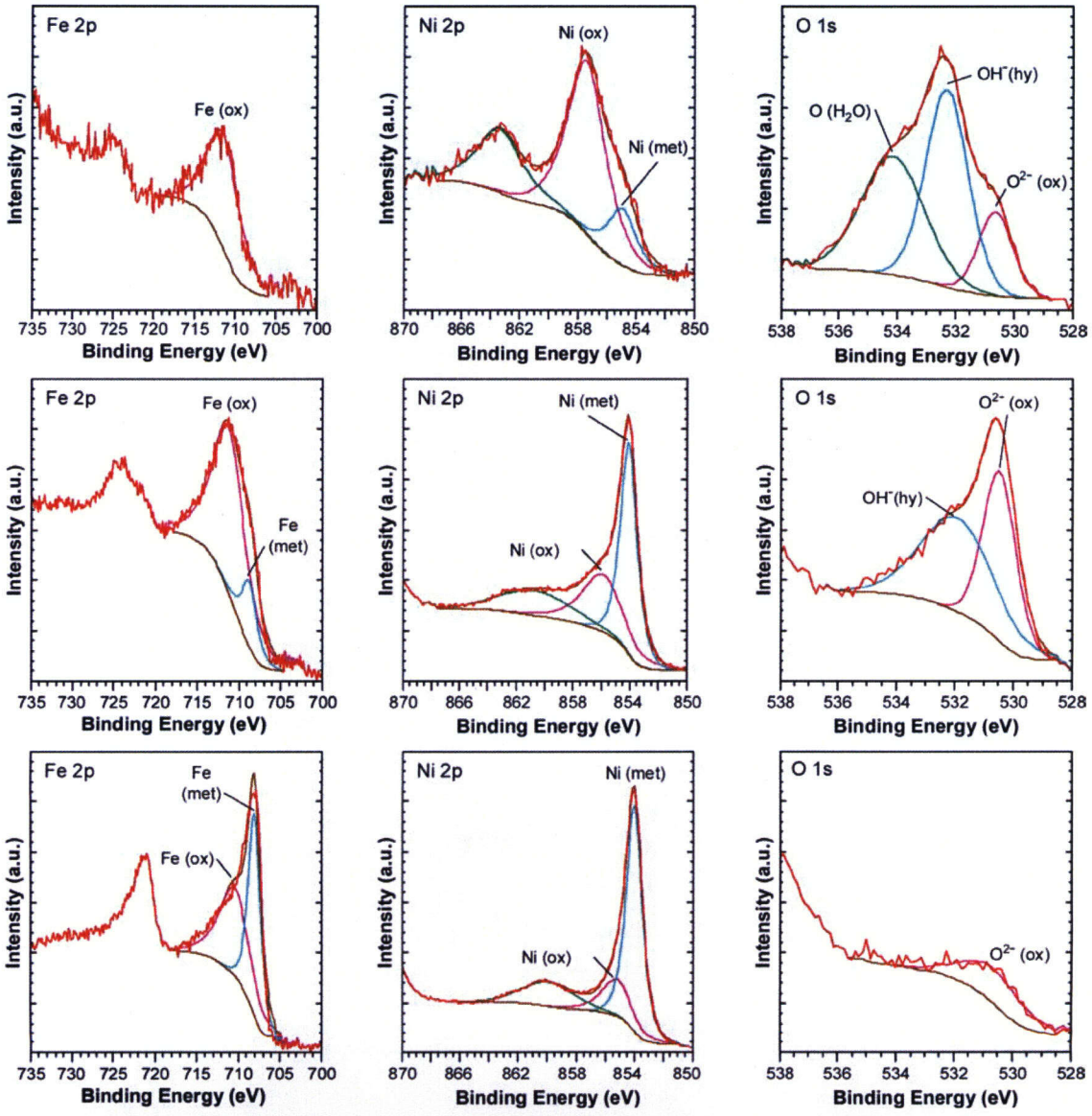

Figure 4-4. High-Resolution Spectrum Curve Fits of the Fe $2p_{3/2}$, Ni $2p_{3/2}$, and O 1s Regions of Josephinite Passivated in Simulated Groundwater at Room Temperature with an Applied Potential of 0 V_{SCE} at pH 12.4 for the As-Received (Top Row) and after Sputtering for 40 Seconds (Middle Row) and for 120 Seconds (Bottom Row)

Table 4-1. Calculated Species Contributions for Various Core-Level Signals of Josephinite Passivated at 0 mV_{SCE} in Simulated Groundwater (pH 12.4) at Room Temperature with an Applied Potential of 0 V_{SCE}				
Sputtering Time (sec)	Equivalent Depth (Å)	Species Contribution		
		Fe $2p_{3/2}$	Ni $2p_{3/2}$	O 1s
0	0	100 Percent Oxide	80 Percent Oxide 20 Percent Metallic	40 Percent H_2O 45 Percent OH^- 15 Percent O^{2-}
40	15	85 Percent Oxide 15 Percent Metallic	40 Percent Oxide 60 Percent Metallic	55 Percent OH^- 45 Percent O^{2-}
120	23	53 Percent Oxide 47 Percent Metallic	23 Percent Oxide 77 Percent Metallic	100 Percent O^{2-}

is low because the oxygen concentration in the base material region was measured to be 3–6 atomic percent. The most profound feature of the species contributions on josephinite is the predominant oxide contribution to the Fe $2p_{3/2}$ core-level signal (85-percent oxide), as well as the hydroxyl contribution to the O 1s signal (55-percent OH^-), in the passive film. The high contribution of iron oxides and hydroxides in the passive film is probably a result of the less noble nature of iron compared to nickel.

Basile, et al. (2000) analyzed the surface of a nickel-iron alloy (75Ni-25Fe in atomic percent) after passivation in boric acid-borate buffer solution (pH 9.2) at 20 °C [68 °F] applying a potential of 200 mV_{SCE}. Results obtained from x-ray photoelectron spectroscopy and Auger electron spectroscopy indicted that the structure of the passive film {10–25 Å [3.94–9.84 × 10^{-5} mils]} is composed of a thin $Ni(OH)_2$ outer layer above a thicker iron oxide inner layer. Rossi, et al. (1992) studied the passive film formed on a 52Ni-48Fe (in atomic percent) alloy in 1 M NaOH solution (pH 13.8) at different potentials. They reported that the passive film also has a duplex structure, but the outer layer was found to be an iron-rich hydroxide and the inner layer a nickel-rich oxide. The outer hydroxide thickness was approximately 12 Å [4.72 × 10^{-5} mils], independent of the applied potential, whereas the inner oxide thickness increased with applied potential up to 60 Å [2.36 × 10^{-4} mils].

According to the indepth profiling concentration measurements in the present investigation, the C_{Ni}/C_{Fe} values observed for josephinite in the passive layer region at pH 12.4 vary from 2.2 at the outer side to 3.0 at the inner side of the film. A similar trend also was observed in the case of pH 9.5. Considering the changes in C_{Ni}/C_{Fe} and the cation contributions to the passive films, it appears the passive film formed on josephinite at 0 mV_{SCE} in simulated groundwater at both pH levels 12.4 and 9.5 also has a duplex structure consisting of an iron-rich hydroxide outer part and a nickel-rich oxide inner part, in agreement with the results reported by Rossi, et al. (1992).

4.2 Comparison with Cast Ni_3Fe Alloy

X-ray photoelectron spectroscopy also was conducted using cast Ni_3Fe alloy samples with a 3-μm [1.18×10^{-4} in] surface finish after identical anodic potentiostatic treatments to that of josephinite in simulated groundwater of pH levels 12.4 and 9.5. As shown in Figure 4-5, the current density versus time plots at both pH levels revealed a fully passive behavior, similar to that shown in Figure 3-10. The steady-state current densities at both pH levels, however, are practically one order of magnitude lower that those plotted in Figure 3-10, presumably caused by the less coarse mechanical polishing allowed for the formation of a more perfect and protective passive film. Contrary to the current density increase observed in the josephinite sample exposed to the pH 9.5 solution (Figure 3.9), the cast Ni_3Fe alloy exhibited a slightly lower current density throughout the polarization period in comparison with that observed in the pH 12.4 solution (Figure 4-5). Frequent current spikes, however, occurred during the whole potentiostatic polarization in the pH 9.5 solution as a result of film breakdown and repassivation events. These current spikes are a signature of metastable pit generation and suggest the cast Ni_3Fe alloy is on the verge of passivity breakdown at the same potential and pH at which pitting initiation already occurred in the josephinite sample. Nevertheless, high pH was also observed to enhance passivity in the cast Ni_3Fe alloy, as shown in Figure 3-6.

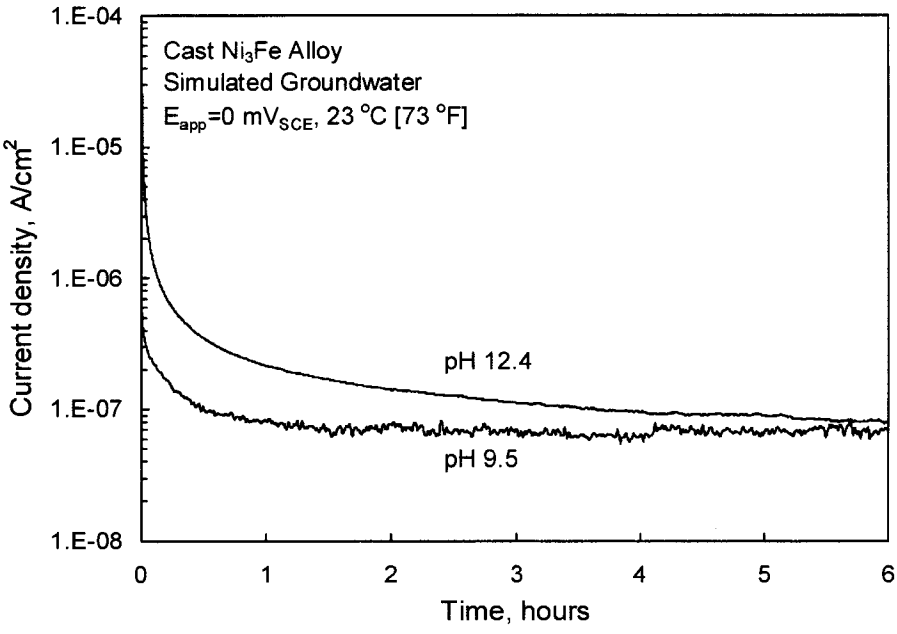

Figure 4-5. Potentiostatic Current Density Versus Time Curves for the Cast Ni_3Fe Alloy, Mechanically Polished to 3-μm [1.18×10^{-4} in] Finish in Simulated Groundwater at Room Temperature with an Applied Potential of 0 V_{SCE} at pH Levels 9.5 and 12.4

Figure 4-6 shows the concentration depth profiles of both passivated cast Ni_3Fe alloy samples. Like the josephinite samples, three distinctive regions with varied chemical compositions were observed. A comparison of the concentration depth profiles for josephinite and the cast Ni_3Fe alloy (Figures 4-2 and 4-6) shows the passive film thickness measured in the samples passivated at pH 12.4 is almost the same. The passive film thickness was observed to decrease slightly in the cast Ni_3Fe alloy by decreasing the pH of the passivating solution to 9.5. The decrease is comparable to that found for josephinite. Additionally, high carbon concentrations were noted near the surface region. Low C_{Ni}/C_{Fe} values were also observed in the passive films formed on both cast Ni_3Fe alloy samples, similar to that in josephinite. These results on the passive film characterization of the cast Ni_3Fe alloy and josephinite using x-ray photoelectron spectroscopy suggest both materials have passive films of similar thickness and composition when subjected to identical environmental and applied potential conditions.

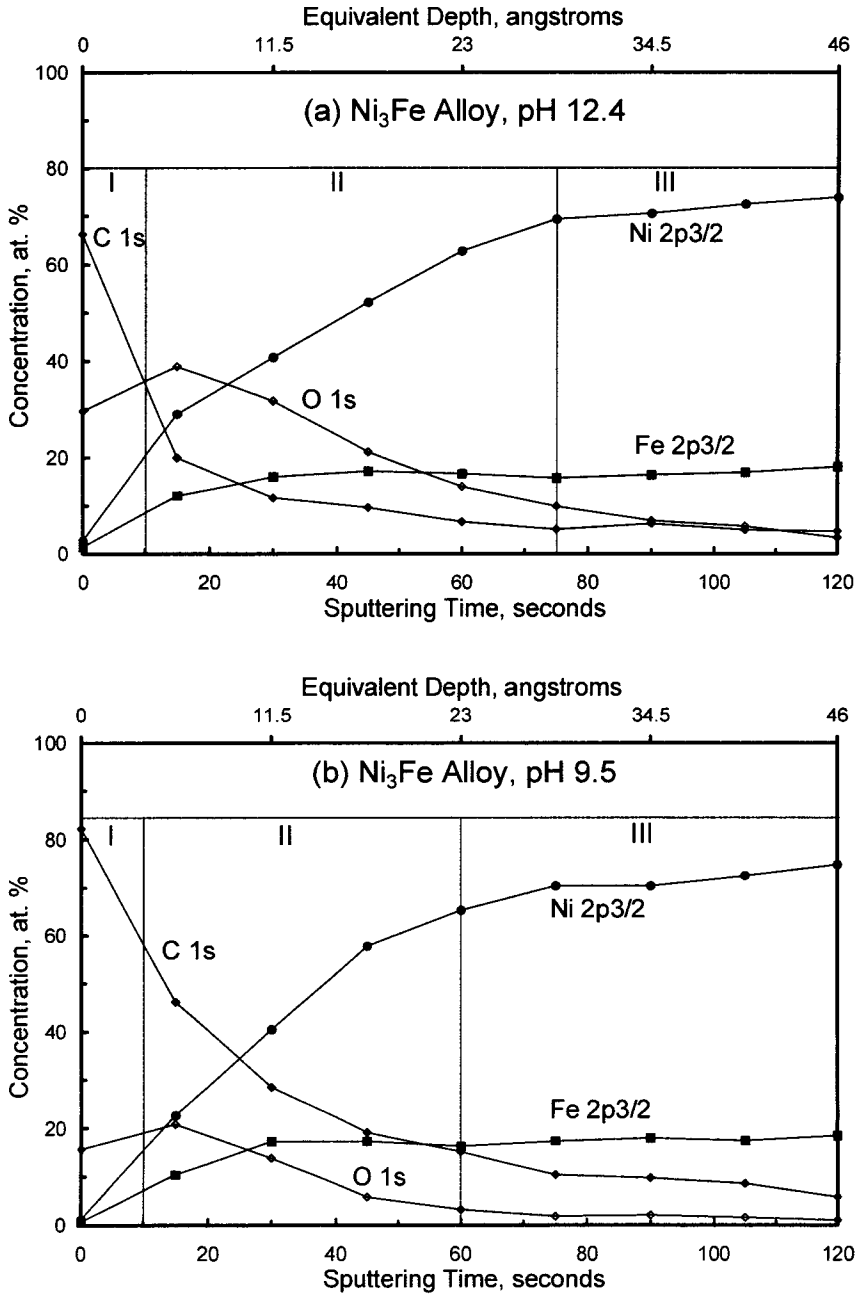

Figure 4-6. Concentration Depth Profiles of Cast Ni_3Fe Alloy Passivated in Simulated Groundwater at Room Temperature with an Applied Potential of 0 V_{SCE} at (a) pH 12.4 and (b) pH 9.5. Equivalent Depth Is Relative to the Sputtering Rate of SiO_2 with the Same Conditions.

5 VALIDITY OF JOSEPHINITE AS A NATURAL ANALOG

In a previous report (Sridhar and Cragnolino, 2002), natural, archeological, and industrial metal analogs were evaluated for their applicability, as one of the multiple lines of evidence, to the assessment of container life. The nickel-chromium-molybdenum alloy proposed to be used as container material has existed only for slightly more than 20 years, and its corrosion behavior is highly dependent on the interplay between material microstructure and environmental conditions. It was noted that the direct use of analogs in estimating the container life in the proposed geologic repository at Yucca Mountain, where both of these factors differ significantly from those of the analogs, is not possible. Because the class of alloys selected as container material depends on a protective oxide film for corrosion resistance, it has been suggested (Sagüés,1999) that natural metallic analogs that have survived for an extraordinarily long time could be useful to reduce concerns regarding the validity of long-term extrapolations when stable passive behavior is assumed. Josephinite was identified by McNeil and Moody (1993) and later by Sagüés (1999) as a natural metal analog deserving further study. The U.S. Department of Energy conducted a limited investigation summarized in Section 1.1. The above suggestions and assessments provide an additional motivation to conduct this investigation in order to assess the validity of josephinite as an appropriate natural metal analog.

Sridhar and Cragnolino (2002) suggested the long-term stability of josephinite metal may be a result of the presence of minor alloying elements, which lend it a specific electrochemical response resulting in long life, or the chemical composition of the environment immediately surrounding josephinite, which may provide conditions for thermodynamic immunity or slow corrosion kinetics.

The present study clearly demonstrates that the anodic behavior of josephinite in slightly alkaline, carbonated water containing anionic species commonly presented in groundwater such as Cl^-, NO_3^-, SO_4^{2-}, and F^-, is similar to that of a synthetic nickel-iron alloy. This alloy was prepared with an almost equivalent chemical composition to that found in the metallic phase of the josephinite sample investigated in this study. Minor differences in the minimum solution pH required to attain stable passivity or marginal differences in the localized corrosion susceptibility, as discussed in Chapter 3, do not indicate a specific electrochemical response of josephinite that could be attributed to minor components of the metallic phase. The main difference in chemical composition and microstructure between the two materials was the presence in the josephinite sample of a secondary intermetallic phase, identified as Ni_3As_2 (see Table 2-7), which was found dispersed in the predominant awaruite phase (see Table 2-6). The presence in the josephinite sample of voids and vugs filled with serpentine introduces another minor difference in the bulk chemical composition between the josephinite and the synthetic alloy (e.g., compare Table 2.5 with Table 3.2). This difference is noted mainly for elements such as silicon, carbon, and oxygen because others are present at much lower concentrations. Nevertheless, these compositional differences, as well as the presence of the Ni_3As_2 secondary phase and the dispersion of serpentine-filled voids and vugs in the metallic matrix, did not lead to significant differences in the anodic behavior, which may help to explain the extremely long-term stability of the josephinite sample collected in the proximity of the Josephine Creek.

It has been reported (Shreir, et al., 1994) that Ni-xFe alloys, in which x varies from 0 to 50 wt%, exhibit corrosion resistance in industrial and marine atmospheres comparable to that of pure nickel. In both fresh and sea waters these alloys are more resistant to general corrosion than iron and mild steel, exhibiting corrosion rates one to two orders of magnitude lower. They are equally susceptible to pitting corrosion with comparable penetration rates. In alternate immersion tests conducted in 5-percent NaCl solutions, values of 0.25, 0.5, and 2.8 $gm^{-2}d^{-1}$ [0.019, 0.038, and 0.21 lb $ft^{-2}yr^{-1}$] were determined for alloys containing 0-, 20- and 63-wt% iron compared with 46 $gm^{-2}d^{-1}$ [3.45 lb $ft^{-2}yr^{-1}$] for pure iron. In another study described by Shreir, et al. (1994), conducted in 3-percent NaCl solutions, the average corrosion rate was 0.1 $gm^{-2}d^{-1}$ [0.008 lb $ft^{-2}yr^{-1}$] for an alloy containing 43-wt% iron, whereas rates more than one order of magnitude higher were found for alloys with 84-percent iron and above. These observations tend to indicate, when compared with results previously discussed for natural and archeological iron analogs, such as iron meteorites (containing between 5- to 10-percent nickel) (Sridhar and Cragnolino, 2002), that josephinite seems to be more resistant to general corrosion than those buried iron-base objects as a result of the presence of nickel, a more noble metal. High nickel content appears to confer an additional resistance to these nickel-base alloys against general corrosion through the formation of a more protective passive film. Nevertheless, the susceptibility to pitting corrosion is not altered significantly. Szklarska-Smialowska (1986) reported the addition of nickel to iron or mild steel increases only slightly the pit initiation potential in chloride solutions.

From the observations previously discussed, it can be concluded that no essential differences exist between josephinite and the cast Ni_3Fe alloy in the anodic behavior and, therefore, on the corrosion resistance in air-saturated aqueous environments. There are no minor alloying elements in josephinite that could provide exceptional corrosion resistance and that may justify the extraordinarily long estimated (or presumed) life of the sample used in this study. It should be noted that these conclusions seem to be valid for humid air and aqueous corrosion at neutral or even slightly acidic or alkaline pH levels, such as those prevailing in industrial and coastal atmospheres or in aqueous media, such as the streams and creeks close to the Josephine Creek, assuming their prevailing pH is that of the Illinois River water (see Table 2-1).

In this context, the second hypothesis regarding the role of the environment immediately surrounding josephinite seems to be a more plausible explanation for the long life of the josephinite sample. It is known, for example, that serpentinization processes produce highly alkaline and reducing conditions (Abrajano, et al., 1988; Kelley, et al., 2001). As clearly demonstrated in the results reported in Chapter 3, both josephinite and the cast Ni_3Fe alloy exhibited a well-defined passive behavior at pH levels above 10.0. Depending on the concentration of Cl^- in the water in contact with josephinite, passivity could be maintained up to extremely high potentials, unattainable with natural corrosion conditions. For example, at pH levels more than 11.0, when the OH^- to Cl^- molar concentration ratio in the simulated groundwater is sufficiently high (i.e., more than 5), pitting corrosion of josephinite is almost completely inhibited. In this case, E_p is too high to be reached in naturally corroding conditions by the corrosion potential in air-saturated solutions. A noticeable hysteresis loop still existed, however, indicating pitting corrosion may occur after prolonged exposures [see Figure 3-2(c)].

At even higher pH levels, the OH^- to Cl^- molar concentration ratio is so high in the simulated groundwater that passivity predominated completely [see Figure 3-2(d)].

According to the plot shown in Figure 3-9, the steady-state passive current density exhibited by josephinite at pH 12.5 is equal to 1.0×10^{-6} A/cm^2 [9.3×10^{-4} A/ft^2]. A uniform corrosion rate of 0.52 gm^{-2}d^{-1} [0.040 lb ft^{-2}yr^{-1}] can be estimated from this value, assuming that Ni_3Fe is the approximate atomic composition of josephinite. This corrosion rate is, however, relatively high to provide an adequate justification for the long-term stability of josephinite (hundreds to millions of years) because it corresponds to a penetration rate of approximately 0.022 mm/yr [0.87 mpy]. The corrosion rates, albeit comparable, are slightly lower for the cast Ni_3Fe alloy. As shown in Figure 3-10, current densities less than 1.0×10^{-6} A/cm^2 [9.3×10^{-4} A/ft^2] can be noted at pH levels 10.0 and 12.5. In addition, current densities one order of magnitude lower were measured on the cast Ni_3Fe alloy when a less coarser finish was used, which was not the case for the josephinite sample.

As discussed in Chapter 3, slight differences exist between josephinite and the cast Ni_3Fe alloy regarding the susceptibility to pitting corrosion in groundwater of relatively low ionic strength. Josephinite was found more susceptible than the cast Ni_3Fe alloy, exhibiting localized corrosion in the cyclic potentiodynamic polarization and potentiostatic tests with environmental conditions (i.e., OH^- to Cl^- molar concentration ratio) in which the synthetic alloy did not experience localized attack. These differences in corrosion resistance, however, are not substantial, and the resistance of josephinite and the synthetic alloy against localized corrosion can be considered similar. In all cases, despite differences in the value of E_p, indicating that josephinite is more susceptible to pitting corrosion, the values of E_{rp} are practically identical in basic saturated water, as shown in Figures 3-3 and 3-8.

Obviously, these arguments are insufficient to explain the extremely long stability of josephinite. X-ray photoelectron spectroscopy was used to analyzed the passive surface layers formed on both the josephinite and the cast Ni_3Fe alloy samples after steady-state potentiostatic polarization in simulated groundwater at potentials in the middle of the passive range (0 V_{SCE}). The passive films were found to have a duplex structure consisting of an iron-rich hydroxide outer layer and an nickel-rich oxide inner layer. The thickness of the passive film is approximately 27 Å [7.48×10^{-8} in] after passivation at pH 12.4 and slightly thinner at pH 9.5. It can be conceived this passive film preceded the formation of protective alteration layers as a result of serpentinization reactions or even acted as a precursor to their formation. No evidence was found to support this hypothesis, however. It should be noted, nevertheless, that, in addition to Mg^{2+} and Ca^{2+}, iron was the prevailing cationic species found in the alteration layer (see Table 2-2) and was also the main component in the outer layer of the passive film. Nickel, essentially confined to the inner passive layer, was present only in a low amount in the alteration layers.

Even though a stable passive film with a definite composition is formed in the josephinite and the cast Ni_3Fe alloy, no evidence was found to support the modeling of the long-term passive behavior of a nickel-chromium-molybdenum alloy on the basis of the point-defect model (Pensado, et al., 2002). For instance, extended evaluation of the josephinite sample did not help to elucidate if voids could have been generated, as postulated in the model, through

coalescence of vacancies at the metallic phase–alteration layer interface after prolonged exposure to a passivating environment.

The difficulties confronted in assessing the validity of josephinite as an adequate analog of a passive, corrosion resistant material such as Alloy 22 can be summarized as follows.

(i) Josephinite does not contain chromium, which is the main alloying element conferring passivity to nickel-chromium-molybdenum alloys. Because the main component of the Alloy 22 passive film is a Cr_2O_3-rich barrier layer, analyses regarding the long-term stability of passive films using josephinite have limitations. This fact was known at the beginning of this investigation. It should be noted in this context, however, the lack of other alloying elements, such as molybdenum and tungsten, that are critical in conferring resistance to localized corrosion to Alloy 22 are not so important to evaluate long-term stable passivity, contrary to what has been claimed (DOE, 2001a).

(ii) Although many aspects regarding the origin and formation of josephinite can be inferred, some of which are still the subject of controversy, it is difficult or almost impossible to elucidate the evolution of the environments contacting josephinite during its formation. This statement refers mostly to the predominantly metallic nickel-iron phase. Nevertheless, many important circumstances not know at the beginning of this study are now reported in Chapter 2.

(iii) Many aspects of the location at which the josephinite was collected are known and, among them, the approximate composition of waters in the region. This information is limited, however, for evaluating the evolution of all the environments that were in contact with the josephinite sample in the location in which it was collected.

The four main benefits of the present study related to the validity of josephinite as an adequate analog are

(i) Characterization of the josephinite sample predominantly as a nickel-iron metallic phase, containing Ni_3As_2 as a minor secondary phase. Whereas the role and importance of the Ni_3Fe phase are clearly understood, the role and relative importance of Ni_3As_2 as a possible contributor to the initiation of pitting corrosion are not yet known.

(ii) Definition of the environmental conditions using pH and groundwater composition, which leads to the passivity of josephinite and the synthetic nickel-iron alloy, and definition of electrochemical conditions that may promote localized corrosion.

(iii) Characterization of the passive film formed on josephinite and the synthetic nickel-iron alloy in groundwater at alkaline pH levels has been completed.

(iv) No evidence of the presence of chlorides in the voids of this mineral was noted in evaluating the possibility of localized corrosion processes in the josephinite sample similar to that reported for iron meteorites (Sridhar and Cragnolino, 2002). Detailed observation of the crack shown in Figure 2-7 did not reveal the presence of pits

associated with localized corrosion in the proximity of the metallic phase–outer alteration layer interface.

A final aspect of importance in the analysis of the josephinite sample is related to the alteration layers found on the outside surface of sample JS–JB1. Formation of these alteration layers may have contributed substantially to the preservation and survival of the metallic core. This speculation can be inferred from the analysis of the crack shown in Figure 2-7. It is possible that this extended crack originated as a result of the serpentinization process occurring on the outer surface of the sample. As indicated by Reaction (2-1), hydrogen (presumably in atomic form) can be generated and evolved as molecular hydrogen (H_2) as a result of the serpentinization reactions. It is also possible, however, that atomic hydrogen is adsorbed on the josephinite surface and then penetrates into the metallic phase, promoting hydrogen embrittlement. As the crack advances, serpentine is continuously formed, exerting a wedging action that may promote the continuous propagation of the crack. It should be noted nickel alloys that exhibit long-range order are more prone to hydrogen embrittlement (Sridhar and Cragnolino, 1992). The existence of long-range order has not been demonstrated in the sample of josephinite used in this study, but it has been reported for Ni_3Fe alloys. This interpretation of the origin of the crack suggests that the alteration layer, mainly composed of serpentine, developed after the nickel-iron metallic phase was formed, thus protecting josephinite from the action of the environment.

It is worthwhile to note that in investigations conducted at the Lawrence Livermore National Laboratory (CRWMS M&O, 2000b), the formation of silicate deposits was detected on metal specimens after exposure to different aqueous environments in the long-term corrosion test facility. By using x-ray diffraction, SiO_2 and NaCl were identified as the main components of the deposits. The largest amount of deposits, however, was found in specimens exposed to simulated acidic water in which the pH is lower than 3.0 and not in alkaline environments. Evaporation experiments conducted in the same laboratory (Rosenberg, et al., 2001) using waters derived from J–13 Well water (see Table 2-1) produced a complete suite of minerals that include amorphous silica (SiO_2), aragonite ($CaCO_3$), calcite ($CaCO_3$), and halite (NaCl), among others. It is impossible to determine with the information available if the deposition of these minerals on metal surfaces may affect the corrosion rate of a passive metal and contribute to the preservation of passivity by coating the passive surface with a highly resistive layer. As expected, there are clear differences among the minerals found in the Lawrence Livermore National Laboratory studies and those identified in the alteration layer of the josephinite sample used in this study.

The possible role of the alteration layers in preserving the stability of josephinite for extremely long times needs to be determined. In particular, the relationship between the passive behavior of the metal surface and the formation of the alteration layers could be critical in understanding the survivability of josephinite.

6 SUMMARY

A sample of josephinite, a rock containing a naturally occurring nickel-iron alloy, was characterized in this study. The exterior of the sample was coated with secondary minerals including the serpentine mineral lizardite, andradite, and the chlorite group mineral clinochlore. The predominant mass of the sample, however, was composed of an intermetallic awaruite phase with a composition close to the stoichiometry of Ni_3Fe. A secondary metallic phase, dispersed in a lower proportion in the nickel-iron phase, was constituted by an arsenic-rich intermetallic with a composition close to Ni_3As_2. The exterior surface of the josephinite sample, exhibited a high density of small voids and vugs filled with serpentine.

Electrochemical characterization studies, comprising of both cyclic potentiodynamic polarization and potentiostatic tests, were conducted using the josephinite sample and a synthetic Ni_3Fe (Ni-23.4 wt% iron) alloy. The tests clearly show that josephinite exhibits an active behavior in a simulated groundwater at pH 8.3. Only at higher pH levels was the stable passivity of josephinite observed. In the pH range 10.0 to 11.9, however, the Cl^- concentration in the simulated groundwater {approximately 0.18 mmol/L [6.4 mg/L]}, though low, was sufficiently high to promote pitting corrosion at relatively low applied potentials. Only at pH 12.8, when the OH^- to Cl^- molar concentration ratio was sufficiently high, was pitting corrosion inhibited. The cast Ni_3Fe exhibits essentially the same behavior, although it was slightly less susceptible to localized corrosion, and stable passivity was attained at lower pH levels.

The passive surface layers that formed on josephinite and the cast Ni_3Fe alloy in simulated groundwater were characterized by x-ray photoelectron spectroscopy combined with indepth sputtering. The objective was to determine, in a comparative fashion, the thickness and chemical composition of the passive films formed on both materials in simulated groundwater of different pH levels after anodic polarization at a potential in the middle of the passive range. It was found that the passive film has a duplex structure consisting of an iron-rich hydroxide outer part and a nickel-rich oxide inner part. The thickness of the passive layer is approximately 27 Å [7.48×10^{-8} in] at pH 12.4 and slightly thinner after passivation at pH 9.5. It can be conceived this passive film preceded the formation of protective alteration layers as a result of serpentinization reactions. No evidence was found to support this hypothesis, however. Even though a stable passive film with a definite composition is formed in josephinite and the cast Ni_3Fe alloy, no evidence was found to support the modeling of the long-term passive behavior of a nickel-chromium-molybdenum alloy based on the extension of the point-defect model to an alloy with three components. For instance, extended evaluation of the josephinite sample did not help to elucidate if voids could have been generated as postulated in the model, through coalescence of vacancies at the metallic phase–alteration layer interface, after prolonged exposure to a passivating environment.

Difficulties in considering josephinite an adequate metal analog for Alloy 22 or corrosion resistant nickel-chromium-molybdenum alloys in general were discussed. Ignoring the absence of chromium as the main alloying element conferring passivity, the lack of knowledge regarding the environment in contact with the josephinite sample throughout its history emerged as the main problem to assess the validity of josephinite as an analog.

Results obtained from this study provide an appropriate characterization of environmental conditions leading to passivity and how localized corrosion could become the main threat to the stability of passive films in conditions found in the proposed repository. The possible role of the alteration layers in preserving the stability of josephinite for extremely long times needs to be determined. In particular, the relationship between the passive behavior of the metal surface and the formation of the alteration layers could be critical in understanding the survivability of josephinite.

7 REFERENCES

Abrajano, T.A., N.C. Sturchio, J.K. Bohlke, G.L. Lyon, R.J. Poreda, and C.M. Stevens. "Methane-Hydrogen Gas Seeps, Zambales Ophiolite, Philippines: Deep or Shallow Origin?" *Chemical Geology* Vol. 71. pp. 211–222. 1988.

ASTM International. "Standard Test Method for Conducting Cyclic Potentiodynamic Polarization Measurements for Localized Corrosion Susceptibility of Iron-, Nickel-, or Cobalt-Based Alloys." *G61–86: Annual Book of Standards. Vol. 3.02: Wear and Erosion—Metal Corrosion.* West Conshohocken, Pennsylvania: ASTM International. pp. 237–241. 1999.

Barnes, I. and J.R. O'Neil. "The Relationship Between Fluids in Some Fresh Alpine-Type Ultramafics and Possible Modern Serpentinization, Western United States." *Geological Society of America Bulletin.* Vol. 80. pp. 1,947–1,960. 1969.

Barnes, I., V.C. LaMarche, Jr., and G. Himmelberg. "Geochemical Evidence of Present Day Serpentinization." *Science.* Vol. 156. pp. 830–832. 1967.

Basile, F., J. Bergner, C. Bombart, B. Rondot, P. Le Guevel, and G. Lorang. "Electrochemical and Analytical (XPS and AES) Study of Passive Layers Formed on Fe-Ni Alloys in Borate Solutions." *Surface and Interface Analysis.* Vol. 30. pp. 154–175. 2000.

Bassett, W.A., J.M. Bird, M.S. Weathers, and D.L. Kohlstedt. "Josephinite: Crystal Structures and Phase Relations of the Metals." *Physics of Earth and Planetary Interiors.* Vol. 23. pp. 255–261. 1980.

Bird, J.M. "The Status of Our Studies of Josephinite and Related Rocks." <http://www.geo.cornell.edu/geology/faculty/Bird.html>. 2001.

Bird, J.M. and M.S. Weathers. "Origin of Josephinite." *Geochemical Journal.* Vol. 13. pp. 41–55. 1979.

———. "Josephinite: Specimens from the Earth's Core." *Earth and Planetary Science Letters.* Vol. 28. pp. 51–64. 1975.

Bird, J.M., A. Meibom, R. Frei, and T.F. Nägler. "Osmium and Lead Isotopes of Rare OsIrRu Minerals: Derivation from the Core–Mantle Boundary Region?" *Earth and Planetary Science Letters.* Vol. 170. pp. 83–92. 1999.

Bird, J.M., W.A. Bassett, and M.S. Weathers. "Windmanstaetten Pattern in Josephinite, a Metal-Bearing Terrestrial Rock." *Science.* Vol. 206. pp. 832–834. 1979.

Bochsler, P., A. Stettler, J.M. Bird, and M.S. Weathers. "Excess ^{3}He and ^{21}Ne in Josephinite." *Earth and Planetary Science Letters.* Vol. 39. pp. 67–74. 1978.

Botto, R.I. and G.H. Morrison. "Josephinite: A Unique Nickel-Iron." *American Journal of Science*. Vol. 276. pp. 241–274. 1976.

CRWMS M&O. "Natural Analogue Synthesis Report". TDR–NBS–GS–00026. Rev. 00 ICN 02. Las Vegas, Nevada: CRWMS M&O. 2002.

———. "Environment on the Surfaces of the Drip Shield and Waste Package Outer Barrier." ANL–EBS–MD–000001. Rev 00 ICN 01. Las Vegas, Nevada: CRWMS M&O. 2000a.

———. "General Corrosion and Localized Corrosion of Waste Package Outer Barrier." ANL–EBS–MD–000003. Rev. 00. Las Vegas, Nevada: TRW Environmental Safety Systems, Inc. 2000b.

Dick, H.J.B. "Terrestrial Nickel-Iron from the Josephine Peridotite, Its Geologic Occurrence, Associations, and Origin." *Earth and Planetary Science Letters*. Vol. 24. pp. 291–298. 1974.

———. "K-Ar Dating of Intrusive Rocks in the Josephine Peridotite and Rogue Formation West of Cave Junction, Southwestern Oregon." *Geological Society of America Abstracts with Programs*. Vol. 5. p. 33. 1973.

Dick, H.J.B. and H. Gillette. "Josephinite: Specimens from the Earth's Core?—A Discussion." *Earth and Planetary Science Letters*. Vol. 31. pp. 308–311. 1976.

DOE. "Technical Update Impact Letter Report." MIS–MGR–RL–000001. Rev. 00 ICN 02. Appendix E. Las Vegas, Nevada: DOE, Office of Civilian Radioactive Waste Management. 2001a.

———. "FY01—Supplemental Science and Performance Analyses. Vol. 1: Scientific Bases and Analyses." TDR–MGR–MD–000007. Rev. 00 ICN 01. Las Vegas, Nevada: DOE, Office of Civilian Radioactive Waste Management. 2001b.

Downing, R.G., E.W. Hennecke, and O.K. Manuel. "Josephinite: A Terrestrial Alloy with a Radiogenic Xenon-129 and Noble Gas Imprint of Iron Meteorites." *Geochemical Journal*. Vol. 11. pp. 219–229. 1977.

Frost, B.R. "On the Stability of Sulfides, Oxides, and Native Metals in Serpentinite." *Journal of Petrology*. Vol. 26. pp. 31–63. 1985.

Heusler, K.E. "Passivity and Breakdown of Passivity of Nickel, Cobalt, and Chromium." *Passivity of Metals*. R.P. Frankenthal and J. Kruger, eds. Princeton, New Jersey: The Electrochemical Society. pp. 771–801. 1978.

Johnson, A.B. and B. Francis. "Durability of Metals from Archeological Objects, Metal Meteorites, and Native Metals." PNL–3198. UC–70. Richland, Washington: Pacific Northwest National Laboratory. 1980.

Kelley, D. J., Karson, D. Blackman, G. Früh-Green, D. Butterfield, M. Lilley, M. Schrenk, E. Olson, K. Roe, J. Lebon, and Shipboard Scientific Party. "Discovery of Lost City: An Off-Axis, Peridotite-Hosted, Hydrothermal Field Near 30 °N on the Mid-Atlantic Ridge." *Newsletter of the US RIDGE Initiative.* Vol. 11, No. 2. pp. 3–9. 2001.

Macdonald, D.D. and D. Owen. "The Electrochemistry of Nickel Metal in Lithium Hydroxide Solutions at 22, 170, and 250 °C." *High Temperature, High Pressure Electrochemistry in Aqueous Solutions.* D. de G. Jones and R.W. Staehle, eds. Houston, Texas: NACE International. pp. 513–523. 1976.

McNeil, M.B. and J.B. Moody. "Corrosion Model Validation in High-Level Nuclear Waste Package Research." Scientific Basis for Nuclear Waste Management XVI. C.G. Interrante and R.T. Pabalan, eds. Symposium Proceedings 294. Pittsburgh, Pennsylvania: Materials Research Society. pp. 549–556. 1993.

Melville, W.H. "Josephinite, A New Nickel-Iron". *American Journal of Science.* Vol. 43. pp. 509–515. 1892.

Miller, W., R. Alexander, N. Chapman, I. McKinley, and J. Smellie. *Geological Disposal of Radioactive Wastes and Natural Analogues.* Amsterdam, The Netherlands: Pergamon. 2000.

Mohanty, S., T.J. McCartin, and D.W. Esh. "Total System Performance Assessment (TPA) Version 4.0 Code: Module Description and Users Guide." San Antonio, Texas: CNWRA. 2000.

Moulder, J.F., W.F. Stickle, P.E. Sobol, and K.D. Bomben. *Handbook of X-Ray Photoelectron Spectroscopy.* Eden Prairie, Minnesota: Perkin-Elmer Corporation. 1992.

Nuclear Waste Technical Review Board. "Report to the U.S. Congress and the U.S. Secretary of Energy." Arlington, Virginia: Nuclear Waste Technical Review Board. 2001.

Organization for Economic Co-Operation and Development/Nuclear Energy Agency-International Atomic Energy Agency. "An International Peer Review of the Yucca Mountain Project Total-System Performance Assessment Supporting Site Recommendation." Paris, France: Organization for Economic Co-Operation and Development Publications. 2002.

Pensado, O., D.S. Dunn, and G.A. Cragnolino. "Passive Dissolution of Container Materials Modeling and Experiments." CNWRA 2003-01. San Antonio, Texas: CNWRA. 2002.

Pourbaix, M. *Atlas of Electrochemical Equilibria in Aqueous Solution.* Houston, Texas: NACE International. 1974.

Qvarfort, R. "New Electrochemical Cell for Pitting Corrosion Testing." *Corrosion Science.* Vol. 28. pp. 135–140. 1988

Ramdohr, P. "Über Josephinit, Awaruit, Souesit, Ihre Eigenschaften, Entstehung Und Paragenesis." *Mineral Magazine.* Vol. 29. pp. 374–394. 1950.

Ramp, L. "Geologic Map of the Northwest Quarter of the Cave Junction Quadrangle, Josephine County, Oregon." Geological Map Series, Map GMS–38. Scale 1:24,000. 1986.

Ramp, L. and N.V. Peterson. *Geology and Mineral Resources of Josephine County, Oregon. Bulletin 100.* Portland, Oregon: State of Oregon Department of Geology and Mineral Industries. 1979.

Rosenberg, N.D., G.E. Gdowdski, and K.G. Knauss. "Evaporative Chemical Evolution of Natural Waters at Yucca Mountain, Nevada." *Applied Geochemistry.* Vol. 16. pp. 1,231–1,240. 2001.

Rossi, A., C. Calinski, H.-W. Hoppe, and H.-H. Strehblow. "A Combined ISS and XPS Investigation of Passive Film Formation on Fe53Ni." *Surface and Interface Analysis.* Vol. 18. pp. 269–276. 1992.

Sagüés, A.A. "Nuclear Waste Package Corrosion Behavior in the Proposed Yucca Mountain Repository." Scientific Basis for Nuclear Waste Management XXII. D.J. Wronkiewics and J.H. Lee, eds. Symposium Proceedings 556. Pittsburgh, Pennsylvania: Materials Research Society. pp. 845–854. 1999.

Shreir, L.L., R.A. Jarman, and G.T. Bursterin. *Corrosion: Metal/Environment Interactions.* Vol. 1. London, United Kingdom: Butherworth-Heinemann. 1994.

Sridhar, N. and G.A. Cragnolino. "Evaluation of Analogs for the Performance Assessment of High-Level Waste Container Materials." CNWRA 2002-03. San Antonio, Texas: CNWRA. 2002.

———. "Stress Corrosion Cracking of Nickel-Base Alloys." *Stress Corrosion Cracking—Materials Performance and Evaluation.* R.H. Jones, ed. Materials Park, Ohio: ASM International. pp. 131–179. 1992.

Szklarska-Smialowska, Z. *Pitting Corrosion of Metals.* Houston, Texas: NACE International. 1986.

Thornber, C.R. and S.E. Haggerty. "Origin and Mineral Chemistry of Josephinite." *Transactions of the American Geophysical Union.* Vol. 57. pp. 355. 1976.